

# Channel Shaping Using Beyond Diagonal Reconfigurable Intelligent Surfaces

Yang Zhao, *Member, IEEE*, Hongyu Li, *Graduate Student Member, IEEE*,  
Massimo Franceschetti, *Fellow, IEEE*, and Bruno Clerckx, *Fellow, IEEE*

**Abstract**—This paper investigates to what extent a passive Reconfigurable Intelligent Surface (RIS) can redistribute the singular values of a Multiple-Input Multiple-Output (MIMO) point-to-point channel. We depart from the conventional diagonal phase shift model and adopt a Beyond-Diagonal (BD)-RIS architecture featuring in-group connections between elements, which enables signal amplitude and phase control. Specifically, we first provide shaping insights by characterizing the Pareto frontiers of channel singular values via a novel geodesic manifold optimization. The resulting region comprehensively encapsulates most relevant metrics (e.g., spectral norm and condition number). To explore the shaping limits of passive BD-RIS, we also derive singular value bounds for 1) rank-deficient forward/backward channel and 2) blocked direct channel. As a side product, we tackle BD-RIS-aided MIMO achievable rate maximization by a local-optimal Alternating Optimization (AO) approach and a suboptimal shaping-inspired design over channel gain maximization. Simulation results show that BD-RIS improves the dynamic range of and trade-off between channel singular values significantly, compared to conventional diagonal RIS. Results also highlight that the power and rate gain of BD-RIS over diagonal RIS increase with MIMO dimensions.

**Index Terms**—Beyond diagonal reconfigurable intelligent surface, multi-input multi-output, manifold optimization, channel shaping, rate maximization.

## I. INTRODUCTION

Today we are witnessing a paradigm shift from connectivity to intelligence, where the wireless environment is no longer a chaotic medium but a conscious agent that can serve on demand. This is empowered by the recent advances in Reconfigurable Intelligent Surface (RIS), a programmable passive planar surface that recycles and redistributes ambient electromagnetic waves for improved wireless performance. A typical RIS consists of numerous low-power sub-wavelength non-resonant scattering elements, whose response can be engineered in real-time to manipulate the amplitude, phase, frequency, and polarization of the scattered waves [1]. It enables low-noise, full-duplex operation, and also features better flexibility than reflectarrays, lighter footprint than relays, and greater scalability than Multiple-Input Multiple-Output (MIMO) systems. The most popular RIS research direction is *joint passive and active beamforming* design with transceivers for a specific performance measure, which has attracted significant attention in wireless communication [2]–[4],

sensing [5]–[7], and power transfer literature [8]–[10]. While passive beamforming at RIS suffers signal attenuation from double fading, it offers better asymptotic behaviors than active beamforming at transceivers (e.g., second-order array gain and fourth-order harvested power [10]). Another RIS application is *backscatter modulation* by periodically switching its reflection pattern within the channel coherence time. This creates a free-ride message stream (similar to index modulation [11]) with dual benefits: integrating with the legacy transmitter for enhanced channel capacity [12]–[14] or serving as an information source for low-power uplink communication [15]–[17]. Different from above, *channel shaping* exploits the RIS as a stand-alone device to modify the inherent properties of the wireless environment. To name a few, it can compensate for the Doppler effect [18], transform frequency-selective channels into frequency-flat [19], improve the spatial diversity for MIMO systems [20], and create artificial time diversity for orthogonal [21] and non-orthogonal [22] multiple accesses. Channel shaping also provides a ubiquitous solution for different wireless applications, which decouples joint RIS-transceiver designs by first optimizing the channel and then the communication system. At a specific resource block, relevant metrics can be classified into two categories:

- *Singular value*: The impact of RIS has been studied in terms of minimum singular value [23], effective rank [23], [24], condition number [25], [26], and degree of freedom [27]–[29]. Those metrics are closely related to performance measures (e.g., achievable rate and harvested power [30]) but sensitive to small perturbations of the channel matrix.
- *Power*: The impact of RIS has been studied in terms of channel power gain [2], [31]–[34] in point-to-point channels and leakage interference [35] in interference channels. Those second-order metrics are less informative in MIMO but easier to analyze and optimize.

Although above works offer initial glimpses into the channel shaping potential of RIS, one critical question has not been fully addressed: *What is the ultimate channel singular value shaping capability of a passive RIS?* The answer depends heavily on RIS hardware architecture and scattering model. Most relevant works [2], [23]–[29], [35] considered a diagonal RIS model where each element is connected to a dedicated impedance and disconnected from others, such that wave impinging on one element is entirely reflected by the same element. This simple architecture ideally maps to a diagonal scattering matrix with unit-magnitude entries on the main diagonal and zeros else-

Yang Zhao, Hongyu Li, and Bruno Clerckx are with the Department of Electrical and Electronic Engineering, Imperial College London, London SW7 2AZ, U.K. (e-mail: {yang.zhao18, c.li21, b.clerckx}@imperial.ac.uk).

Massimo Franceschetti is with the Department of Electrical and Computer Engineering, University of California at San Diego, La Jolla CA 92093, USA (e-mail: massimo@ece.ucsd.edu).

where, which only applies a phase shift to the incoming signal. The concept was then generalized to Beyond-Diagonal (BD)-RIS with a group-connected architecture [31] that connects adjacent elements via passive reconfigurable components<sup>1</sup>. This allows wave impinging on one element to propagate losslessly within the circuit and depart partially from any element in the same group. It can thus manipulate both amplitude and phase of the scattered wave, generalizing the scattering matrix from diagonal to block-diagonal with unitary blocks. Such a powerful model can be realized at reduced hardware cost using tree- and forest-connected architectures according to graph theory [33]. BD-RIS can also function in hybrid transmitting-and-reflecting mode [37] and multi-sector mode [38] to provide full-space coverage and multi-user support. Many practical BD-RIS design challenges, including channel estimation [39], mutual coupling [40], and wideband modelling [41], have also been investigated in the literature. The passive beamforming superiority of BD-RIS over diagonal RIS has been studied mainly in Single-Input Single-Output (SISO) and Multiple-Input Single-Output (MISO) communication systems, where the problems have been cast as single-user Signal-to-Noise Ratio (SNR) maximization [31]–[34] and multi-user Weighted Sum-Rate (WSR) maximization [38], [42]–[44]. However, the interplay between BD-RIS and MIMO systems is still in the infancy stage. The authors of [45] investigated the rate-optimal joint beamforming design for a BD-RIS-aided MIMO system with blocked direct link and fully-connected BD-RIS. Those assumptions simplify the problem but limit the generality of the results. A transmitter-side BD-RIS was introduced to massive MIMO systems for improved spectral efficiency [46], but the problem was again limited to blocked direct link and fully-connected BD-RIS. Received power maximization with continuous-valued [32] and discrete-valued [47] BD-RIS have also been tackled in the literature, but the resulting single-stream transceiver is rate-suboptimal and the corresponding BD-RIS design is equivalent to SISO shaping. We notice that there lacks a comprehensive study of BD-RIS in point-to-point MIMO systems — the shaping benefits of BD-RIS are not fully understood and the general rate maximization problem remains open. Moreover, no previous work has characterized the MIMO channel singular value region manipulated by any type of RIS. This paper aims to narrow those gaps and provide a comprehensive answer to the channel shaping capability question through theoretical analysis and numerical optimization. The contributions are summarized below.

First, we interpret the channel shaping potential of BD-RIS in MIMO as channel rearrangement and space alignment. Channel rearrangement refers to rearranging and recombining the forward and backward channel branches (i.e., entries of the channel matrix) according to their strength. Space alignment generalizes phase matching in SISO and MISO to the high-dimensional singular vector space in MIMO. The off-diagonal entries of BD-RIS scattering matrix provides a higher design freedom and exploits channel spatial diversity

more effectively than diagonal RIS. This is the first paper to study BD-RIS in general MIMO systems.

Second, we propose an efficient BD-RIS design framework that solves general optimization problems (e.g., singular value redistribution and rate maximization) by geodesic<sup>2</sup> Riemannian Conjugate Gradient (RCG). This method modified from [48], [49] exploits the Riemannian geometry of the Stiefel manifold and performs group-wise multiplicative rotational updates along the geodesics, which avoids retraction and facilitates step size selection. It thus converges faster than existing non-geodesic approaches [50], [51]. This is the first work to tailor an efficient optimization framework for BD-RIS.

Third, we adopt the proposed geodesic RCG and provide a numerical answer to the singular value shaping question. The Pareto frontiers of channel singular values are characterized by solving a series of weighted sum maximization problems, where the weight associated with each singular value can be positive, zero, or negative. The enclosed region generalizes most relevant metrics and provides an intuitive channel shaping benchmark. Results show that increasing BD-RIS group size enlarges the singular value region, improving both dynamic range of and trade-off between singular values.

Fourth, we leverage matrix analysis tools and provide an analytical answer to the singular value shaping question. Asymptotic channel singular value bounds applying to diagonal and BD-RIS are derived for rank-deficient forward/backward channel. On the other hand, tight bounds for fully-connected BD-RIS with finite number of elements are derived for blocked direct channel. Results validate those bounds and emphasizes the shaping advantage of BD-RIS. This is the first work to quantify the singular value redistribution capability of BD-RIS from either numerical or analytical perspective.

Fifth, we tackle BD-RIS-aided MIMO rate maximization problem by two beamforming solutions: a local-optimal Alternating Optimization (AO) approach and a low-complexity approach inspired by channel shaping insights. The former updates active beamforming by eigenmode transmission and passive beamforming by proposed geodesic RCG until convergence. The latter suboptimally decouples the problem as channel power gain maximization at BD-RIS and conventional MIMO transmission at transceiver, then solves both in closed form. Results show that BD-RIS provides higher power gain and achievable rate than diagonal RIS, and the rate gap of two approaches diminishes as the BD-RIS evolves from single-connected to fully-connected. It suggests channel shaping offers a promising path to decouple joint RIS-transceiver designs.

*Notation:* Italic, bold lower-case, and bold upper-case letters indicate scalars, vectors and matrices, respectively.  $j$  denotes the imaginary unit.  $\mathbb{C}$  represents the set of complex numbers.  $\mathbb{H}^{n \times n}$  and  $\mathbb{U}^{n \times n}$  denotes the set of  $n \times n$  Hermitian and unitary matrices, respectively.  $\mathbf{0}$  and  $\mathbf{I}$  are the all-zero and identity matrices with appropriate size, respectively.  $\Re\{\cdot\}$  takes the real part of a complex number.  $\arg(\cdot)$  gives the argument of a complex number.  $\text{tr}(\cdot)$  and  $\det(\cdot)$  evaluates the trace and determinant of a square matrix, respectively.

<sup>1</sup>Those components can be either symmetric (e.g., capacitors and inductors) or asymmetric (e.g., ring hybrids and branch-line hybrids) [36], resulting in symmetric and asymmetric scattering matrices, respectively.

<sup>2</sup>A geodesic refers to the shortest path between two points in a Riemannian manifold.

$\text{diag}(\cdot)$  constructs a square matrix with arguments on the main (block) diagonal and zeros elsewhere.  $\text{sv}(\cdot)$  returns the singular value vector.  $\sigma_n(\cdot)$  and  $\lambda_n(\cdot)$  is the  $n$ -th largest singular value and eigenvalue, respectively.  $(\cdot)^*$ ,  $(\cdot)^T$ ,  $(\cdot)^H$ ,  $(\cdot)^\dagger$ ,  $(\cdot)^{(r)}$ ,  $(\cdot)^*$  denote the conjugate, transpose, conjugate transpose (Hermitian), Moore-Penrose inverse,  $r$ -th iterated point, and stationary point, respectively.  $(\cdot)_{[x:y]}$  is a shortcut for  $(\cdot)_x, (\cdot)_{x+1}, \dots, (\cdot)_y$ .  $|\cdot|$ ,  $\|\cdot\|$ , and  $\|\cdot\|_F$  denote the absolute value, Euclidean norm, and Frobenius norm, respectively.  $\odot$  represents the element-wise (Hadamard) product.  $\mathcal{CN}(\mathbf{0}, \mathbf{\Sigma})$  is the multivariate Circularly Symmetric Complex Gaussian (CSCG) distribution with mean  $\mathbf{0}$  and covariance  $\mathbf{\Sigma}$ .  $\sim$  means “distributed as”.

## II. BD-RIS MODEL

Consider a BD-RIS aided point-to-point MIMO system with  $N_T$  and  $N_R$  transmit and receive antennas, respectively, and  $N_S$  scattering elements at the BD-RIS. This configuration is denoted as  $N_T \times N_S \times N_R$  in the following context. The BD-RIS can be modeled as an  $N_S$ -port network [52] that further divides into  $G$  individual groups, each containing  $L \triangleq N_S/G$  elements interconnected by real-time reconfigurable components [31]. To simplify the analysis and explore the performance limits, we assume a lossless asymmetric network without mutual coupling between scattering elements, as previously considered in [37], [38], [45]. The overall scattering matrix of the BD-RIS is block-unitary<sup>3</sup>

$$\mathbf{\Theta} = \text{diag}(\mathbf{\Theta}_1, \dots, \mathbf{\Theta}_G), \quad (1)$$

where  $\mathbf{\Theta}_g \in \mathbb{U}^{L \times L}$  is the  $g$ -th unitary block (i.e.,  $\mathbf{\Theta}_g^H \mathbf{\Theta}_g = \mathbf{I}$ ) that describes the response of group  $g \in \mathcal{G} \triangleq \{1, \dots, G\}$ . Note that diagonal RIS can be regarded as its extreme case with group size  $L=1$ . Some potential physical architectures of BD-RIS are illustrated in [31, Fig. 3], [38, Fig. 5], and [33, Fig. 2], where the circuit topology is modelled in the scattering matrix.

Let  $\mathbf{H}_D \in \mathbb{C}^{N_R \times N_T}$ ,  $\mathbf{H}_B \in \mathbb{C}^{N_R \times N_S}$ ,  $\mathbf{H}_F \in \mathbb{C}^{N_S \times N_T}$  denote the direct (i.e., transmitter-receiver), backward (i.e., RIS-receiver), and forward (i.e., transmitter-RIS) channels, respectively. The equivalent channel is a function of the scattering matrix

$$\mathbf{H} = \mathbf{H}_D + \mathbf{H}_B \mathbf{\Theta} \mathbf{H}_F = \mathbf{H}_D + \sum_g \underbrace{\mathbf{H}_{B,g} \mathbf{\Theta}_g \mathbf{H}_{F,g}}_{\triangleq \mathbf{H}_g}, \quad (2)$$

where  $\mathbf{H}_{B,g} \in \mathbb{C}^{N_R \times L}$  and  $\mathbf{H}_{F,g} \in \mathbb{C}^{L \times N_T}$  are the backward and forward channels for RIS group  $g$ , corresponding to the  $(g-1)L+1$  to  $gL$  columns of  $\mathbf{H}_B$  and rows of  $\mathbf{H}_F$ , respectively. Let  $\mathbf{H}_g \triangleq \mathbf{H}_{B,g} \mathbf{\Theta}_g \mathbf{H}_{F,g}$  be the indirect channel via BD-RIS group  $g$ . Since unitary matrices constitute an algebraic group with respect to multiplication, the scattering matrix of group  $g$  can be decomposed as

$$\mathbf{\Theta}_g = \mathbf{L}_g \mathbf{R}_g^H, \quad (3)$$

where  $\mathbf{L}_g, \mathbf{R}_g \in \mathbb{U}^{L \times L}$  are two unitary factor matrices. Let  $\mathbf{H}_{B,g} = \mathbf{U}_{B,g} \mathbf{\Sigma}_{B,g} \mathbf{V}_{B,g}^H$  and  $\mathbf{H}_{F,g} = \mathbf{U}_{F,g} \mathbf{\Sigma}_{F,g} \mathbf{V}_{F,g}^H$  be

<sup>3</sup>Following footnote 1, we do not assume the scattering matrix to be symmetric. If required, one can enforce symmetry over the block-unitary result by  $\mathbf{\Theta} \leftarrow (\mathbf{\Theta} + \mathbf{\Theta}^T)/2$ .

the compact Singular Value Decomposition (SVD) of the backward and forward channels, respectively. The equivalent channel can thus be rewritten as

$$\mathbf{H} = \mathbf{H}_D + \sum_g \underbrace{\mathbf{U}_{B,g} \mathbf{\Sigma}_{B,g} \mathbf{V}_{B,g}^H}_{\text{backward-forward}} \underbrace{\mathbf{V}_{F,g} \mathbf{\Sigma}_{F,g} \mathbf{U}_{F,g}^H}_{\text{direct-indirect}}. \quad (4)$$

By analyzing (4), we conclude that the off-diagonal entries of the BD-RIS scattering matrix provide two key potentials for MIMO channel shaping:

- *Channel rearrangement*: It refers to rearranging and recombining the backward and forward channel branches (i.e., entries of the channel matrix) associated with each group by their strength. In SISO, diagonal RIS with perfect phase matching provides a maximum indirect channel amplitude of  $\sum_{n=1}^{N_S} |h_{B,n}| |h_{F,n}|$  while BD-RIS can generalize it to  $\sum_{g=1}^G \sum_{l=1}^L |h_{B,\pi_{B,g}(l)}| |h_{F,\pi_{F,g}(l)}|$ , where  $\pi_{B,g}$  and  $\pi_{F,g}$  are permutations of  $\mathcal{L} \triangleq \{1, \dots, L\}$ . Note the first summation is over groups and the second summation is over permuted channels. We thus conclude that BD-RIS exploits spatial diversity effectively thanks to in-group connections. By rearrangement inequality, the maximum channel gain is attained by pairing the  $l$ -th strongest backward and forward branches. Since the number of channels associated with each group is proportional to  $N_T N_R$ , we conclude the advantage of BD-RIS in channel rearrangement scales with MIMO dimensions.
- *Space alignment*: It refers to aligning the singular vectors of the direct, forward, and backward channels. The BD-RIS needs to strike a balance between the alignment of backward-forward (intra-group, multiplicative) channels and direct-indirect (inter-group, additive) channels. In SISO, singular vectors become scalars and space alignment boils down to phase matching, such that the optimal scattering matrix of group  $g$  that maximizes the channel gain is

$$\mathbf{\Theta}_g^* = \exp(j \arg(h_D)) \mathbf{V}_{B,g} \mathbf{U}_{F,g}^H, \quad (5)$$

where  $\mathbf{V}_{B,g} = [\mathbf{h}_{B,g}/\|\mathbf{h}_{B,g}\|, \mathbf{N}_{B,g}] \in \mathbb{U}^{L \times L}$ ,  $\mathbf{U}_{F,g} = [\mathbf{h}_{F,g}/\|\mathbf{h}_{F,g}\|, \mathbf{N}_{F,g}] \in \mathbb{U}^{L \times L}$ , and  $\mathbf{N}_{B,g}, \mathbf{N}_{F,g} \in \mathbb{C}^{L \times (L-1)}$  are the orthonormal bases of the null spaces of  $\mathbf{h}_{B,g}$  and  $\mathbf{h}_{F,g}$ , respectively. Diagonal RIS with empty null space thus suffices for perfect phase matching in SISO. When it comes to MIMO, element  $g$  of diagonal RIS can only apply a common phase shift to the “pinhole”<sup>4</sup> indirect channel passing through itself by  $\mathbf{H}_g = \mathbf{h}_{B,g} \mathbf{\Theta}_g \mathbf{h}_{F,g}^H \in \mathbb{C}^{N_R \times N_T}$ . That is, the disadvantage of diagonal RIS in space alignment scales with MIMO dimensions.

## III. BD-RIS DESIGN BY GEODESIC RCG

Most group-connected BD-RIS design problems can be formulated in the following general form

$$\max_{\mathbf{\Theta}} f(\mathbf{\Theta}) \quad (6a)$$

$$\text{s.t.} \quad \mathbf{\Theta}_g^H \mathbf{\Theta}_g = \mathbf{I}, \quad \forall g, \quad (6b)$$

<sup>4</sup>The pinhole effect refers to channel rank reduction due to diffraction in the propagation environment [53]. For element  $g$  of diagonal RIS, the indirect channel  $\mathbf{H}_g$  is rank-1 and the pinhole is  $\mathbf{\Theta}_g$ .

where the objective function  $f(\Theta)$  can be any function of the BD-RIS scattering matrix  $\Theta$ , for example, channel singular value (to be discussed in Section IV) and achievable rate (to be discussed in Section V). The feasible domain of each group is a  $L$ -dimensional Stiefel manifold  $\Theta_g \in \mathbb{U}^{L \times L}$ , which is non-convex and non-Euclidean. Therefore, relevant optimization problems are usually solved by relax-then-project methods [42] or universal non-geodesic manifold RCG [37], [38], [45]. The former solves an unconstrained problem (6a) by quasi-Newton methods, then projects the solution back to the Stiefel manifold. It has no guarantee of optimality and may suffer from numerical instability. The latter generalizes the conjugate gradient methods to any Riemannian manifold, which updates the feasible point by progressing along the conjugate direction and projecting back to the manifold at each step. In the following context, we first discuss the existing non-geodesic RCG method and its drawbacks, then propose a novel group-wise geodesic RCG method that operates directly on the Stiefel manifold for faster convergence.

#### A. Non-Geodesic RCG

A geodesic is a curve representing the shortest path between two points in a Riemannian manifold, whose tangent vectors remain parallel when transporting along the curve. The universal RCG method proposed in [50], [51] is non-geodesic and applicable to optimization problems over arbitrary manifolds. The main idea is to perform additive updates along the conjugate direction guided by the Riemannian gradient, then project the solution back onto the manifold. For optimization problem (6), the steps for BD-RIS group  $g$  at iteration  $r$  are summarized below:

- 1) *Compute the Euclidean gradient* [54]: The gradient of  $f$  with respect to  $\Theta_g^*$  in the Euclidean space is

$$\nabla_{\mathbf{E},g}^{(r)} = \frac{\partial f(\Theta_g^{(r)})}{\partial \Theta_g^*}; \quad (7)$$

- 2) *Translate to the Riemannian gradient* [50]: At point  $\Theta^{(r)}$ , the Riemannian gradient lies in the tangent space of the Stiefel manifold  $\mathcal{T}_{\Theta_g^{(r)}} \mathbb{U}^{L \times L} \triangleq \{\mathbf{M} \in \mathbb{C}^{L \times L} \mid \mathbf{M}^H \Theta_g^{(r)} + \Theta_g^{(r)H} \mathbf{M} = \mathbf{0}\}$ . It gives the steepest ascent direction of the objective on the manifold can be obtained by projecting the Euclidean gradient onto the tangent space:

$$\nabla_{\mathbf{R},g}^{(r)} = \nabla_{\mathbf{E},g}^{(r)} - \Theta_g^{(r)} \nabla_{\mathbf{E},g}^{(r)H} \Theta_g^{(r)}; \quad (8)$$

- 3) *Determine the conjugate direction* [55]: The conjugate direction is obtained over the Riemannian gradient and previous direction as

$$\mathbf{D}_g^{(r)} = \nabla_{\mathbf{R},g}^{(r)} + \gamma_g^{(r)} \mathbf{D}_g^{(r-1)}, \quad (9)$$

where  $\gamma_g^{(r)}$  is the parameter that deviates the conjugate direction from the tangent space for accelerated convergence. A popular choice is the Polak-Ribière formula

$$\gamma_g^{(r)} = \frac{\text{tr}((\nabla_{\mathbf{R},g}^{(r)} - \nabla_{\mathbf{R},g}^{(r-1)}) \nabla_{\mathbf{R},g}^{(r)H})}{\text{tr}(\nabla_{\mathbf{R},g}^{(r-1)} \nabla_{\mathbf{R},g}^{(r-1)H})}; \quad (10)$$

- 4) *Perform additive update* [51]: The point is updated by moving along a straight path in the conjugate direction

$$\bar{\Theta}_g^{(r+1)} = \Theta_g^{(r)} + \mu \mathbf{D}_g^{(r)}, \quad (11)$$

where  $\mu$  is the step size refinable by the Armijo rule [56];

- 5) *Retract for feasibility* [37], [50]: The resulting point needs to be projected to the closest point (in terms of Euclidean distance) on the Stiefel manifold by

$$\Theta_g^{(r+1)} = \bar{\Theta}_g^{(r+1)} (\bar{\Theta}_g^{(r+1)H} \bar{\Theta}_g^{(r+1)})^{-1/2}. \quad (12)$$

One can also combine the addition (11) and retraction (12) in one step

$$\Theta_g^{(r+1)} = (\Theta_g^{(r)} + \mu \mathbf{D}_g^{(r)}) (\mathbf{I} + \mu^2 \mathbf{D}_g^{(r)H} \mathbf{D}_g^{(r)})^{-1/2}, \quad (13)$$

and determine the step size therein.

The above method is called non-geodesic since the points are updated in the linear embedding spaces by addition (11) and retraction (12), instead of on the Stiefel manifold itself. It converges to stationary points of the original problem but usually requires a large number of iterations due to inefficient operations in the Euclidean space.

#### B. Geodesic RCG

Before introducing geodesic RCG, we revisit some basic concepts in differential geometry and Lie algebra. A Lie group is simultaneously a continuous group and a differentiable manifold. Lie algebra refers to the tangent space of the Lie group at the identity element. The exponential map acts as a bridge between the Lie algebra and Lie group, which allows one to recapture the local group structure using linear algebra techniques. The set of unitary matrices  $\mathbb{U}^{L \times L}$  forms a Lie group  $U(L)$  under multiplication, and the corresponding Lie algebra  $\mathfrak{u}(L) \triangleq \mathcal{T}_{\mathbf{I}} \mathbb{U}^{L \times L} = \{\mathbf{M} \in \mathbb{C}^{L \times L} \mid \mathbf{M}^H + \mathbf{M} = \mathbf{0}\}$  consists of skew-Hermitian matrices. A geodesic emanating from the identity with velocity  $\mathbf{D} \in \mathfrak{u}(L)$  can be described by [57]

$$\mathbf{G}_{\mathbf{I}}(\mu) = \exp(\mu \mathbf{D}), \quad (14)$$

where  $\exp(\mathbf{A}) = \sum_{k=0}^{\infty} (\mathbf{A}^k / k!)$  is the matrix exponential and  $\mu$  is the step size (i.e., magnitude of the tangent vector). Note that the right translation is an isometry in  $U(L)$ . During the optimization of group  $g$ , the geodesic evaluated at the identity (14) should be translated to  $\Theta_g^{(r)}$  for successive updates [48]

$$\mathbf{G}_g^{(r)}(\mu) = \mathbf{G}_{\mathbf{I}}(\mu) \Theta_g^{(r)} = \exp(\mu \mathbf{D}_g^{(r)}) \Theta_g^{(r)}, \quad (15)$$

while the Riemannian gradient evaluated at  $\Theta_g^{(r)}$  (8) should be translated back to the identity for exploiting the Lie algebra [48]

$$\tilde{\nabla}_{\mathbf{R},g}^{(r)} = \nabla_{\mathbf{R},g}^{(r)} \Theta_g^{(r)H} = \nabla_{\mathbf{E},g}^{(r)} \Theta_g^{(r)H} - \Theta_g^{(r)} \nabla_{\mathbf{E},g}^{(r)H}. \quad (16)$$

After gradient translation, the deviation parameter and conjugate direction can be determined similarly to (10) and (9)

$$\tilde{\gamma}_g^{(r)} = \frac{\text{tr}((\tilde{\nabla}_{\mathbf{R},g}^{(r)} - \tilde{\nabla}_{\mathbf{R},g}^{(r-1)}) \tilde{\nabla}_{\mathbf{R},g}^{(r)H})}{\text{tr}(\tilde{\nabla}_{\mathbf{R},g}^{(r-1)} \tilde{\nabla}_{\mathbf{R},g}^{(r-1)H})}. \quad (17)$$

$$\mathbf{D}_g^{(r)} = \tilde{\nabla}_{\mathbf{R},g}^{(r)} + \tilde{\gamma}_g^{(r)} \mathbf{D}_g^{(r-1)}, \quad (18)$$

---

**Algorithm 1:** Group-wise geodesic RCG for BD-RIS design
 

---

**Input:**  $f(\Theta)$ ,  $G$ **Output:**  $\Theta^*$ 

```

1: Initialize  $r \leftarrow 0$ ,  $\Theta^{(0)}$ 
2: Repeat
3:   For  $g \leftarrow 1$  to  $G$ 
4:      $\nabla_{E,g}^{(r)} \leftarrow (7)$ 
5:      $\tilde{\nabla}_{R,g}^{(r)} \leftarrow (16)$ 
6:      $\tilde{\gamma}_g^{(r)} \leftarrow (17)$ 
7:      $\mathbf{D}_g^{(r)} \leftarrow (18)$ 
8:     If  $\Re\{\text{tr}(\mathbf{D}_g^{(r)\text{H}} \tilde{\nabla}_{R,g}^{(r)})\} < 0$   $\triangleright$  not an ascent direction
9:        $\mathbf{D}_g^{(r)} \leftarrow \tilde{\nabla}_{R,g}^{(r)}$ 
10:    End If
11:     $\mu \leftarrow 1$ 
12:     $\mathbf{G}_g^{(r)}(\mu) \leftarrow (15)$ 
13:    While  $f(\mathbf{G}_g^{(r)}(2\mu)) - f(\Theta_g^{(r)}) \geq \mu \cdot \text{tr}(\mathbf{D}_g^{(r)} \mathbf{D}_g^{(r)\text{H}})/2$ 
14:       $\mu \leftarrow 2\mu$ 
15:    End While
16:    While  $f(\mathbf{G}_g^{(r)}(\mu)) - f(\Theta_g^{(r)}) < \mu/2 \cdot \text{tr}(\mathbf{D}_g^{(r)} \mathbf{D}_g^{(r)\text{H}})/2$ 
17:       $\mu \leftarrow \mu/2$ 
18:    End While
19:     $\Theta_g^{(r+1)} \leftarrow (19)$ 
20:  End For
21:   $r \leftarrow r+1$ 
22: Until  $|f(\Theta^{(r)}) - f(\Theta^{(r-1)})|/f(\Theta^{(r-1)}) \leq \epsilon$ 

```

---

The solution can thus be updated along the geodesic in a multiplicative rotational manner

$$\Theta_g^{(r+1)} = \mathbf{G}_g^{(r)}(\mu) = \exp(\mu \mathbf{D}_g^{(r)}) \Theta_g^{(r)}, \quad (19)$$

where an appropriate  $\mu$  may be obtained by the Armijo rule. To double the step size, one can simply square the rotation matrix instead of recomputing the matrix exponential, since  $\exp^2(\mu \mathbf{D}_g^{(r)}) = \exp(2\mu \mathbf{D}_g^{(r)})$ .

Algorithm 1 summarizes the proposed BD-RIS design framework based on group-wise geodesic RCG. Compared to the non-geodesic approach, it leverages the Lie group properties to replace the add-then-retract update (13) with a multiplicative rotational update (19) along the geodesic. This leads to faster convergence and simplifies the step size tuning thanks to appropriate parameter space. Convergence to a local optimum is still guaranteed if not initialized at a stationary point. Note that the group-wise updates can be performed in parallel to facilitate large-scale BD-RIS optimization problems. Since block-unitary matrices are also closed under multiplication, one can avoid group-wise updates by directly operating on  $\Theta$  and pinching (i.e., keeping the block diagonal and nulling the other entries) the Euclidean gradient (7), with potentially higher computational complexity and slower convergence.

#### IV. CHANNEL SINGULAR VALUES REDISTRIBUTION

In this section, we first provide a toy example to illustrate the channel shaping advantage of BD-RIS architecture. Next, we numerically characterize the channel singular value region based on the proposed Algorithm 1. Finally, we derive some analytical singular value bounds in specific scenarios.

##### A. Toy Example

We first illustrate the channel shaping capabilities of different RIS models by a toy example. Consider a  $2 \times 2 \times 2$

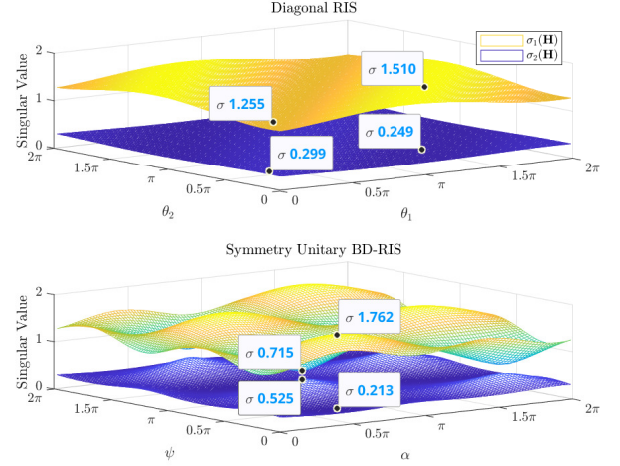


Fig. 1.  $2 \times 2 \times 2$  (no direct) channel singular value shaping by diagonal RIS and symmetric fully-connected BD-RIS.

setup where the direct link is blocked. The diagonal RIS is modeled by  $\Theta_D = \text{diag}(e^{j\theta_1}, e^{j\theta_2})$  while the fully-connected BD-RIS has 4 independent angular parameters

$$\Theta_U = e^{j\phi} \begin{bmatrix} e^{j\alpha} \cos \psi & e^{j\beta} \sin \psi \\ -e^{-j\beta} \sin \psi & e^{-j\alpha} \cos \psi \end{bmatrix}. \quad (20)$$

It is worth noting that  $\phi$  has no impact on the singular value because  $\text{sv}(e^{j\phi} \mathbf{A}) = \text{sv}(\mathbf{A})$ . To simplify the analysis, we also enforce symmetry  $\Theta_U = \Theta_U^T$  by  $\beta = \pi/2$  such that both architectures have the same number of variables in the scattering matrix. Fig. 1 compares the achievable singular values of one typical channel realization, where the direct channel is blocked and the forward and backward channels are normalized Rayleigh fading

$$\mathbf{H}_B = \begin{bmatrix} -0.2059 + 0.5914j & -0.0909 + 0.5861j \\ 0.4131 + 0.2651j & -0.1960 + 0.4650j \end{bmatrix},$$

$$\mathbf{H}_F = \begin{bmatrix} -0.6362 + 0.1332j & -0.1572 + 1.5538j \\ 0.0196 + 0.4011j & -0.3170 - 0.2303j \end{bmatrix}.$$

The results are obtained by an exhaustive grid search over  $(\theta_1, \theta_2)$  for diagonal RIS and  $(\alpha, \psi)$  for symmetric fully-connected BD-RIS. In this example, we observe that both singular values can be manipulated up to <sup>5</sup> 9% by diagonal RIS (using 2 reconfigurable impedances) and 42% by symmetric fully-connected BD-RIS (using 3 reconfigurable impedances). The extra performance gain comes purely from connecting both scattering elements, and a larger gain is expected an asymmetric reconfigurable component is available. This example shows that BD-RIS can provide a wider dynamic range of channel singular values and motivates further studies on channel shaping.

##### B. Pareto Frontier Characterization

We then characterize the Pareto frontier of singular values of a general  $N_T \times N_S \times N_R$  channel (2) by maximizing their

<sup>5</sup>The percentage for manipulating the  $n$ -th channel singular value is calculated by  $\eta_n = \frac{\max \sigma_n(\mathbf{H}) - \min \sigma_n(\mathbf{H})}{2\sigma_n(\mathbf{H})} \times 100\%$ . In this case, we notice  $\eta_1 = \eta_2$  for both RIS architectures.

weighted sum

$$\max_{\Theta} \sum_n \rho_n \sigma_n(\mathbf{H}) \quad (21a)$$

$$\text{s.t. } \Theta_g^H \Theta_g = \mathbf{I}, \quad \forall g, \quad (21b)$$

where  $n \in \mathcal{N} \triangleq \{1, \dots, N\}$ ,  $N \triangleq \min(N_T, N_R)$  is the maximum channel rank, and  $\rho_n$  is the weight of the  $n$ -th singular value that can be positive, zero, or negative. Varying  $\{\rho_n\}_{n \in \mathcal{N}}$  characterizes the Pareto frontier that encloses the entire singular value region. Thus, we claim problem (21) generalizes most singular value shaping problems. It can be solved optimally by Algorithm 1 with the Euclidean gradient given by Lemma 1.

**Lemma 1.** *The Euclidean gradient of (21a) with respect to BD-RIS group  $g$  is*

$$\frac{\partial \sum_n \rho_n \sigma_n(\mathbf{H})}{\partial \Theta_g^*} = \mathbf{H}_{B,g}^H \mathbf{U} \text{diag}(\rho_1, \dots, \rho_N) \mathbf{V}^H \mathbf{H}_{F,g}^H, \quad (22)$$

where  $\mathbf{U}$  and  $\mathbf{V}$  are the left and right compact singular matrices of  $\mathbf{H}$ , respectively.

*Proof.* Please refer to Appendix A.  $\square$

We then analyze the computational complexity of solving Pareto singular value problem (21) by Algorithm 1. To update each BD-RIS group, compact SVD of  $\mathbf{H}$  requires  $\mathcal{O}(NN_T N_R)$ , Euclidean gradient (22) requires  $\mathcal{O}(LN(N_T + N_R + L + 1))$ , Riemannian gradient translation (16) requires  $\mathcal{O}(L^3)$ , deviation parameter (17) and conjugate direction (18) together require  $\mathcal{O}(L^2)$ , and matrix exponential (19) requires  $\mathcal{O}(L^3)$  operations [58]. The overall complexity is thus  $\mathcal{O}(I_{\text{RCG}}G(NN_T N_R + LN(N_T + N_R + L + 1) + I_{\text{BLS}}L^3))$ , where  $I_{\text{RCG}}$  and  $I_{\text{BLS}}$  are the number of iterations for geodesic RCG and backtracking line search (line 13–18 of Algorithm 1), respectively.

### C. Some Analytical Bounds

We then discuss some analytical bounds related to channel singular values, which help us to explore and understand the channel shaping limits of passive RIS.

Degree of Freedom (DoF) (a.k.a. multiplexing gain) refers to the maximum number of independent streams that can be transmitted in parallel over a MIMO channel, which is defined as

$$d = \lim_{\rho \rightarrow \infty} \frac{\log \det(\mathbf{I} + \rho \mathbf{H} \mathbf{H}^H)}{\log \rho}, \quad (23)$$

where  $\rho$  is the SNR.

**Proposition 1** (Degree of freedom). *In point-to-point MIMO, BD-RIS cannot achieve a higher DoF than diagonal RIS.*

*Proof.* Please refer to Appendix B.  $\square$

**Proposition 2** (Rank-deficient channel). *If the minimum rank of forward and backward channels is  $k$  ( $k \leq N$ ), then for diagonal RIS or BD-RIS of arbitrary number of elements, the  $n$ -th singular value of the equivalent channel is bounded above and below respectively by*

$$\sigma_n(\mathbf{H}) \leq \sigma_{n-k}(\mathbf{T}), \quad \text{if } n > k, \quad (24a)$$

$$\sigma_n(\mathbf{H}) \geq \sigma_n(\mathbf{T}), \quad \text{if } n < N - k + 1, \quad (24b)$$

where  $\mathbf{T}$  is an auxiliary matrix satisfying

$$\mathbf{T} \mathbf{T}^H = \begin{cases} \mathbf{H}_D(\mathbf{I} - \mathbf{V}_F \mathbf{V}_F^H) \mathbf{H}_D^H, & \text{if } \text{rank}(\mathbf{H}_F) = k, \\ \mathbf{H}_D^H(\mathbf{I} - \mathbf{U}_B \mathbf{U}_B^H) \mathbf{H}_D, & \text{if } \text{rank}(\mathbf{H}_B) = k, \end{cases} \quad (25)$$

and  $\mathbf{V}_F$  and  $\mathbf{U}_B$  are the right and left compact singular matrices of  $\mathbf{H}_F$  and  $\mathbf{H}_B$ , respectively.

*Proof.* Please refer to Appendix C.  $\square$

Inequality (24a) states that if the forward and backward channels are at least rank  $k$ , then the  $n$ -th singular value of  $\mathbf{H}$  can be enlarged to the  $(n-k)$ -th singular value of  $\mathbf{T}$ , or suppressed to the  $n$ -th singular value of  $\mathbf{T}$ . Moreover, the first  $k$  channel singular values are unbounded above<sup>6</sup> while the last  $k$  channel singular values can be suppressed to zero. An example is given in Corollary 2.1 for Line-of-Sight (LoS) channels (i.e.,  $k=1$ )<sup>7</sup>.

**Corollary 2.1** (LoS channel). *If the forward or backward channel is LoS, then a diagonal RIS or BD-RIS can at most enlarge the  $n$ -th ( $n \geq 2$ ) channel singular value to the  $(n-1)$ -th singular value of  $\mathbf{T}$ , or suppress the  $n$ -th channel singular value to the  $n$ -th singular value of  $\mathbf{T}$ . That is,*

$$\sigma_1(\mathbf{H}) \geq \sigma_1(\mathbf{T}) \geq \sigma_2(\mathbf{H}) \geq \dots \geq \sigma_{N-1}(\mathbf{T}) \geq \sigma_N(\mathbf{H}) \geq \sigma_N(\mathbf{T}). \quad (26)$$

*Proof.* This is a direct result of (24) with  $k=1$ .  $\square$

We would like to highlight that Proposition 2 holds for both diagonal and BD-RIS with arbitrary number of elements, regardless of the presence of direct channel. The bounds are asymptotically tight when the number of scattering elements approaches infinity. On the other hand, we will show in Section VI that with a finite number of elements, BD-RIS can approach those bounds better than diagonal RIS. Proposition 2 evaluates the ultimate channel shaping limits of passive RIS and provides a selection guideline for scattering element number in a practical deployment scenario.

**Proposition 3** (Blocked direct channel). *If the direct link is blocked and the BD-RIS is fully-connected, then the channel singular values can be manipulated up to*

$$\text{sv}(\mathbf{H}) = \text{sv}(\mathbf{B}\mathbf{F}), \quad (27)$$

where  $\mathbf{B}$  and  $\mathbf{F}$  are arbitrary matrices with  $\text{sv}(\mathbf{B}) = \text{sv}(\mathbf{H}_B)$  and  $\text{sv}(\mathbf{F}) = \text{sv}(\mathbf{H}_F)$ .

*Proof.* Please refer to Appendix D.  $\square$

Proposition 3 states that if the direct channel is blocked and the BD-RIS is fully-connected, the only singular value bounds on the equivalent channel are the singular value bounds on the product of unitary-transformed forward and backward channels. For example, consider a  $2 \times 2 \times 2$  setup with

$$\mathbf{H}_B = \begin{bmatrix} 3 & 0 \\ 0 & 2 \end{bmatrix}, \quad \mathbf{H}_F = \begin{bmatrix} 1 & 0 \\ 0 & 4 \end{bmatrix}.$$

<sup>6</sup>The energy conservation law  $\sum_n \sigma_n^2(\mathbf{H}) \leq 1$  still has to be respected. This constraint is omitted in the following context for brevity.

<sup>7</sup>We notice a similar eigenvalue result has been derived in [59] but is limited to diagonal RIS.

It is apparent that any diagonal RIS can only achieve singular values  $\text{sv}(\mathbf{H}) = [8, 3]^\top$ , but a fully connected BD-RIS with  $\Theta = \begin{bmatrix} 0 & 1 \\ 1 & 0 \end{bmatrix}$  can achieve  $\text{sv}(\mathbf{H}) = [12, 2]^\top$ . That is, fully-connected BD-RIS applies right unitary transformation on  $\mathbf{H}_B$  and left unitary transformation on  $\mathbf{H}_F$ , widening the singular values to  $8 \leq \sigma_1(\mathbf{H}) \leq 12$  and  $2 \leq \sigma_2(\mathbf{H}) \leq 3$ .

Proposition 3 transforms the shaping capacity question to a mathematical one, namely how the singular values of matrix product are bounded by the singular values of its individual factors. Let  $\bar{N} = \max(N_T, N_S, N_R)$  and  $\sigma_n(\mathbf{H}) = \sigma_n(\mathbf{H}_F) = \sigma_n(\mathbf{H}_B) = 0$  for  $N < n \leq \bar{N}$ . We have the following corollaries.

**Corollary 3.1** (Generic singular value bounds).

$$\prod_{k \in K} \sigma_k(\mathbf{H}) \leq \prod_{i \in I} \sigma_i(\mathbf{H}_B) \prod_{j \in J} \sigma_j(\mathbf{H}_F), \quad (28)$$

for all admissible triples  $(I, J, K) \in T_r^{\bar{N}}$  with  $r < \bar{N}$ , where

$$\begin{aligned} T_r^{\bar{N}} &\triangleq \left\{ (I, J, K) \in U_r^{\bar{N}} \mid \forall p < r, (F, G, H) \in T_p^r, \right. \\ &\quad \left. \sum_{f \in F} i_f + \sum_{g \in G} j_g \leq \sum_{h \in H} k_h + p(p+1)/2 \right\}, \\ U_r^{\bar{N}} &\triangleq \left\{ (I, J, K) \mid \sum_{i \in I} i + \sum_{j \in J} j = \sum_{k \in K} k + r(r+1)/2 \right\}. \end{aligned}$$

*Proof.* Please refer to [60, Theorem 8].  $\square$

Corollary (3.1) is by far the most comprehensive singular value bound over Proposition 3, which is also recognized as a variation of Horn's inequality [61]. It is worth mentioning that the number of admissible triples (and bounds) grows exponentially with  $\bar{N}$ . For example, the number of inequalities described by (28) grows from 12 to 2062 when  $\bar{N}$  increases from 3 to 7. This renders the analytic approach computationally expensive for large-scale MIMO systems. Next, we showcase some useful inequalities enclosed by (28). Readers are referred to [62, Chapter 16, 24] for more examples.

**Corollary 3.2** (Upper bound on the largest singular value).

$$\sigma_1(\mathbf{H}) \leq \sigma_1(\mathbf{H}_B) \sigma_1(\mathbf{H}_F). \quad (29)$$

*Proof.* This is a direct result of (28) with  $r = 1$ .  $\square$

**Corollary 3.3** (Lower bound on the smallest singular value).

$$\sigma_{\bar{N}}(\mathbf{H}) \geq \sigma_{\bar{N}}(\mathbf{H}_B) \sigma_{\bar{N}}(\mathbf{H}_F). \quad (30)$$

*Proof.* This can be deduced from (28) with  $r_1 = \bar{N} - 1$  and  $r_2 = \bar{N}$ .  $\square$

**Corollary 3.4** (Upper bound on the product of first  $k$  singular values).

$$\prod_{n=1}^k \sigma_n(\mathbf{H}) \leq \prod_{n=1}^k \sigma_n(\mathbf{H}_B) \prod_{n=1}^k \sigma_n(\mathbf{H}_F). \quad (31)$$

*Proof.* This is a direct result of (28) with  $r = k$ .  $\square$

**Corollary 3.5** (Lower bound on the product of last  $k$  singular values).

$$\prod_{n=\bar{N}}^{\bar{N}-k+1} \sigma_n(\mathbf{H}) \geq \prod_{n=\bar{N}}^{\bar{N}-k+1} \sigma_n(\mathbf{H}_B) \prod_{n=\bar{N}}^{\bar{N}-k+1} \sigma_n(\mathbf{H}_F). \quad (32)$$

*Proof.* This can be deduced from (28) with  $r_1 = \bar{N} - k$  and  $r_2 = \bar{N}$ .  $\square$

Corollaries 3.3 and 3.5 are less informative when  $\bar{N} \neq N$  (i.e., unequal number of transmit and receive antennas and scattering elements) as the lower bounds would coincide at zero.

**Corollary 3.6** (Upper bound on the channel power gain). *The channel power gain is upper bounded by the sum of sorted element-wise product of squared singular values of backward and forward channels*

$$\|\mathbf{H}\|_F^2 = \sum_{n=1}^N \sigma_n^2(\mathbf{H}) \leq \sum_{n=1}^N \sigma_n^2(\mathbf{H}_B) \sigma_n^2(\mathbf{H}_F). \quad (33)$$

*Proof.* Please refer to [62, Inequality 24.4.7].  $\square$

To achieve the equalities in Corollaries (3.2) – (3.6), the RIS needs to completely align the spaces of  $\mathbf{H}_B$  and  $\mathbf{H}_F$ . The resulting scattering matrix is generally required to be unitary

$$\Theta^* = \mathbf{V}_B \mathbf{U}_F^H, \quad (34)$$

which can be concluded from (52) and (53) in Appendix D. Interestingly, diagonal RIS can attain those equalities if and only if  $\mathbf{H}_B$  and  $\mathbf{H}_F$  are both rank-1. In such case, the equivalent channel reduces to  $\mathbf{H} = \sigma_B \sigma_F \mathbf{u}_B \mathbf{v}_B^H \Theta \mathbf{u}_F \mathbf{v}_F^H$  and the RIS only needs to align  $\mathbf{v}_B^H$  and  $\mathbf{u}_F$  by

$$\Theta^* = \mathbf{v}_B \mathbf{u}_F^H \odot \mathbf{I}, \quad (35)$$

which becomes a special case of (5). On the other hand, when  $\mathbf{H}_B$  and  $\mathbf{H}_F$  are both in Rayleigh fading, the expected maximum channel power gain  $\mathbb{E}\{\|\mathbf{H}\|_F^2\}_{\max}$  can be evaluated as

$$\sum_{n=1}^N \int_0^\infty f_{\lambda_n^{\min(N_R, N_S)}}(x_n) dx_n \int_0^\infty f_{\lambda_n^{\min(N_S, N_T)}}(x_n) dx_n, \quad (36)$$

where  $\lambda_n^K$  is the  $n$ -th eigenvalue of the complex  $K \times K$  Wishart matrix with probability density function  $f_{\lambda_n^K}(x_n)$  given by [63, Equation 51]. We notice (36) is a generalization of [31, Equation 58] to MIMO.

Proposition 3 and Corollaries 3.2 – 3.6 provide a comprehensive answer to singular value bounds and channel power gain limits for fully-connected BD-RIS with blocked direct channel. Tight bounds are inapplicable in more general cases since the direct-indirect channels and backward-forward channels cannot be completely aligned at the same time. In such case, we can exploit optimization approaches from a singular value perspective (Section IV-B) or a power gain perspective (Section V-A).

## V. POWER GAIN AND ACHIEVABLE RATE MAXIMIZATION

### A. Channel Power Gain

The MIMO channel power gain maximization problem is formulated with respect to the BD-RIS scattering matrix

$$\max_{\Theta} \quad \|\mathbf{H}_D + \mathbf{H}_B \Theta \mathbf{H}_F\|_F^2 \quad (37a)$$

$$\text{s.t.} \quad \Theta_g^H \Theta_g = \mathbf{I}, \quad \forall g, \quad (37b)$$

which generalizes the case of SISO [31], MISO [34], [42], single-stream MIMO [32], [47], and direct link-blocked MIMO



with fully-connected BD-RIS (34). The key of solving (37) is to balance the additive and multiplicative space alignments.

**Remark 1.** Interestingly, in terms of maximizing the inner product  $\langle \mathbf{H}_D, \mathbf{H}_B \mathbf{\Theta} \mathbf{H}_F \rangle$ , (37) is reminiscent of the weighted orthogonal Procrustes problem [64]

$$\min_{\mathbf{\Theta}} \quad \|\mathbf{H}_D - \mathbf{H}_B \mathbf{\Theta} \mathbf{H}_F\|_F^2 \quad (38a)$$

$$\text{s.t.} \quad \mathbf{\Theta}^H \mathbf{\Theta} = \mathbf{I}, \quad (38b)$$

which relaxes the block-unitary constraint (38b) to unitary but still has no trivial solution. One lossy transformation exploits the Moore-Penrose inverse and moves  $\mathbf{\Theta}$  to one side of the product [65], formulating two standard orthogonal Procrustes problems

$$\min_{\mathbf{\Theta}} \quad \|\mathbf{H}_B^\dagger \mathbf{H}_D - \mathbf{\Theta} \mathbf{H}_F\|_F^2 \text{ or } \|\mathbf{H}_D \mathbf{H}_F^\dagger - \mathbf{H}_B \mathbf{\Theta}\|_F^2 \quad (39a)$$

$$\text{s.t.} \quad \mathbf{\Theta}^H \mathbf{\Theta} = \mathbf{I}, \quad (39b)$$

which have global optimal solutions

$$\mathbf{\Theta} = \mathbf{U} \mathbf{V}^H, \quad (40)$$

where  $\mathbf{U}$  and  $\mathbf{V}$  are respectively the left and right compact singular matrices of  $\mathbf{H}_B^\dagger \mathbf{H}_D \mathbf{H}_F^\dagger$  or  $\mathbf{H}_B^\dagger \mathbf{H}_D \mathbf{H}_F^\dagger$  [66]. We emphasize that (34) and (40) are valid fully-connected BD-RIS solutions to (37) when the direct link is blocked and present, but the latter is neither optimal nor a generalization of the former due to the lossy transformation.

Inspired by [67], we propose an optimal solution to problem (37) with arbitrary group size. The idea is to successively approximate the quadratic objective (37a) by local Taylor expansions and solve each step in closed form by group-wise SVD.

**Proposition 4.** Starting from any feasible  $\mathbf{\Theta}^{(0)}$ , the sequence

$$\mathbf{\Theta}_g^{(r+1)} = \mathbf{U}_g^{(r)} \mathbf{V}_g^{(r)}, \quad \forall g. \quad (41)$$

converges to a stationary point of (37), where  $\mathbf{U}_g^{(r)}$  and  $\mathbf{V}_g^{(r)}$  are the left and right compact singular matrices of

$$\mathbf{M}_g^{(r)} = \mathbf{H}_{B,g}^H \left( \mathbf{H}_D + \mathbf{H}_B \text{diag}(\mathbf{\Theta}_{[1:g-1]}^{(r+1)}, \mathbf{\Theta}_{[g:G]}^{(r)}) \mathbf{H}_F \right) \mathbf{H}_{F,g}^H \quad (42)$$

*Proof.* Please refer to Appendix F.  $\square$

We then analyze the computational complexity of solving channel gain maximization problem (37) by Proposition 4. To update each BD-RIS group, matrix multiplication (42) requires  $\mathcal{O}(N_T N_R + (G+1)(NL^2 + N_T N_R L))$  operations and its compact SVD requires  $\mathcal{O}(L^3)$  operations. The overall complexity is thus  $\mathcal{O}(I_{\text{SAA}} G (N_T N_R + (G+1)(NL^2 + N_T N_R L) + L^3))$ , where  $I_{\text{SAA}}$  is the number iterations for successive affine approximation.

## B. Achievable Rate Maximization

We aim to maximize the achievable rate of the BD-RIS-aided MIMO system by jointly optimizing the active and passive beamforming

$$\max_{\mathbf{W}, \mathbf{\Theta}} \quad R = \log \det \left( \mathbf{I} + \frac{\mathbf{W}^H \mathbf{H}^H \mathbf{H} \mathbf{W}}{\eta} \right) \quad (43a)$$

$$\text{s.t.} \quad \|\mathbf{W}\|_F^2 \leq P, \quad (43b)$$

$$\mathbf{\Theta}_g^H \mathbf{\Theta}_g = \mathbf{I}, \quad \forall g, \quad (43c)$$

where  $\mathbf{W}$  is the transmit precoder,  $R$  is the achievable rate,  $\eta$  is the average noise power, and  $P$  is the transmit power constraint. Problem (43) is non-convex due to the block-unitary constraint (43c) and the coupling between variables. We propose a local-optimal approach via AO and a low-complexity approach based on channel shaping.

1) *Alternating Optimization:* This approach updates  $\mathbf{\Theta}$  and  $\mathbf{W}$  iteratively until convergence. For a given  $\mathbf{W}$ , the passive beamforming subproblem is

$$\max_{\mathbf{\Theta}} \quad \log \det \left( \mathbf{I} + \frac{\mathbf{H} \mathbf{Q} \mathbf{H}^H}{\eta} \right) \quad (44a)$$

$$\text{s.t.} \quad \mathbf{\Theta}_g^H \mathbf{\Theta}_g = \mathbf{I}, \quad \forall g, \quad (44b)$$

where  $\mathbf{Q} \triangleq \mathbf{W} \mathbf{W}^H$  is the transmit covariance matrix. Problem (44) can be solved optimally by Algorithm 1 with the Euclidean gradient given by Lemma 2.

**Lemma 2.** The Euclidean gradient of (44a) with respect to BD-RIS block  $g$  is

$$\frac{\partial R}{\partial \mathbf{\Theta}_g^*} = \frac{1}{\eta} \mathbf{H}_{B,g}^H \left( \mathbf{I} + \frac{\mathbf{H} \mathbf{Q} \mathbf{H}^H}{\eta} \right)^{-1} \mathbf{H} \mathbf{Q} \mathbf{H}_{F,g}^H. \quad (45)$$

*Proof.* Please refer to Appendix E.  $\square$

For a given  $\mathbf{\Theta}$ , the global optimal transmit precoder is given by eigenmode transmission [68]

$$\mathbf{W}^* = \mathbf{V} \text{diag}(\mathbf{s}^*)^{1/2}, \quad (46)$$

where  $\mathbf{V}$  is the right singular matrix of the equivalent channel and  $\mathbf{s}^*$  is the optimal water-filling power allocation obtainable by the iterative method [69].

The AO algorithm is guaranteed to converge to local-optimal points of problem (43) since each subproblem is solved optimally and the objective is bounded above. Similar to the analysis in Section IV-B, the computational complexity of solving subproblem (44) by geodesic RCG is  $\mathcal{O}(I_{\text{RCG}} G (NL^2 + LN_T N_R + N_T^2 N_R + N_T N_R^2 + N_R^3 + I_{\text{BLS}} L^3))$ . On the other hand, the complexity of solving active beamforming subproblem by (46) is  $\mathcal{O}(N N_T N_R)$ . The overall complexity is thus  $\mathcal{O}(I_{\text{AO}} (I_{\text{RCG}} G (NL^2 + LN_T N_R + N_T^2 N_R + N_T N_R^2 + N_R^3 + I_{\text{BLS}} L^3) + N N_T N_R))$ , where  $I_{\text{AO}}$  is the number of iterations for AO.

2) *Low-Complexity Solution:* We then propose a suboptimal two-stage solution to problem (43) that decouples the joint RIS-transceiver design. The idea is to first consider channel shaping and replace the rate maximization subproblem (44) by channel power gain maximization problem (37), then proceed to conventional eigenmode transmission (46). Both steps are



TABLE I  
AVERAGE PERFORMANCE OF GEODESIC AND NON-GEODESIC RCG ALGORITHMS ON PROBLEM (21)

RCG path	$N_S = 16$			$N_S = 256$		
	Objective	Iterations	Time [s]	Objective	Iterations	Time [s]
Geodesic	$4.359 \times 10^{-3}$	11.59	$1.839 \times 10^{-2}$	$1.163 \times 10^{-2}$	25.58	3.461
Non-geodesic	$4.329 \times 10^{-3}$	30.92	$5.743 \times 10^{-2}$	$1.116 \times 10^{-2}$	61.40	13.50

solved in closed form and the computational complexity is  $\mathcal{O}(I_{\text{SAA}}G(N_T N_R + (G+1)(NL^2 + N_T N_R L) + L^3) + NN_T N_R)$ . While suboptimal, this shaping-inspired solution avoids outer iterations and implements inner iterations more efficiently.

## VI. SIMULATION RESULTS

In this section, we provide numerical results to evaluate the proposed BD-RIS designs. Consider a distance-dependent path loss model  $\Lambda(d) = \Lambda_0 d^{-\gamma}$  where  $\Lambda_0$  is the reference path loss at distance 1 m,  $d$  is the propagation distance, and  $\gamma$  is the path loss exponent. The small-scale fading model is  $\mathbf{H} = \sqrt{\kappa/(1+\kappa)}\mathbf{H}_{\text{LoS}} + \sqrt{1/(1+\kappa)}\mathbf{H}_{\text{NLoS}}$ , where  $\kappa$  is the Rician  $K$ -factor,  $\mathbf{H}_{\text{LoS}}$  is the deterministic LoS component, and  $\mathbf{H}_{\text{NLoS}} \sim \mathcal{CN}(\mathbf{0}, \mathbf{I})$  is the Rayleigh component. We set  $\Lambda_0 = -30\text{dB}$ ,  $d_D = 14.7\text{m}$ ,  $d_F = 10\text{m}$ ,  $d_B = 6.3\text{m}$ ,  $\gamma_D = 3$ ,  $\gamma_F = 2.4$  and  $\gamma_B = 2$  for reference, which corresponds to a typical indoor environment with  $\Lambda_D = -65\text{dB}$ ,  $\Lambda_F = -54\text{dB}$ ,  $\Lambda_B = -46\text{dB}$ . The indirect path via RIS is thus 35 dB weaker than the direct path. Rayleigh fading (i.e.,  $\kappa=0$ ) is assumed for all channels unless otherwise specified.

### A. Algorithm Evaluation

We first compare in Table I the geodesic and non-geodesic RCG algorithm on problem (21) in an  $N_T = N_S = 4$  system with BD-RIS group size  $L=4$ . The statistics are averaged over 100 independent runs. It is observed that the geodesic RCG method achieves a slightly higher objective value with significantly (up to  $3\times$ ) lower number of iterations and shorter (up to  $4\times$ ) computational time than the non-geodesic method. The results demonstrate the efficiency of the proposed geodesic RCG algorithm especially in large-scale BD-RIS design problems.

### B. Channel Singular Values Redistribution

1) *Pareto Frontier*: Fig. 2 shows the Pareto singular values of an  $N_T = N_R = 2$  MIMO reshaped by a RIS. When the direct link is blocked, the achievable regions in Fig. 2(a) are shaped like pizza slices. This is because  $\sigma_1(\mathbf{H}) \geq \sigma_2(\mathbf{H}) \geq 0$  and there exists a trade-off between the alignment of two spaces. We observe that the smallest singular value can be enhanced up to  $2 \times 10^{-4}$  by single-connected RIS and  $3 \times 10^{-4}$  by fully-connected BD-RIS, corresponding to a 50 % gain. When the direct link is present, the shape of the singular value region depends heavily on the relative strength of the indirect link. In Fig. 2(b), a 32-element RIS is insufficient to compensate the 35 dB path loss imbalance and results in a limited singular value region that is symmetric around the direct point. As the group size  $L$  increases, the shape of the region evolves from

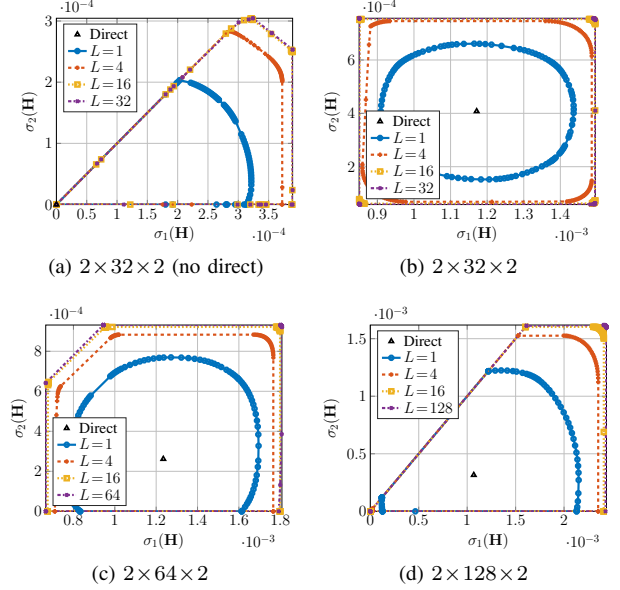


Fig. 2. Pareto frontiers of singular values of an  $N_T = N_R = 2$  channel reshaped by a RIS.

elliptical to square. This transformation not only improves the dynamic range of  $\sigma_1(\mathbf{H})$  and  $\sigma_2(\mathbf{H})$  by 22 % and 38 %, but also provides a better trade-off in manipulating both singular values. It suggests the design freedom from larger group size allows better alignment of multiple spaces simultaneously. The singular value region also enlarges as the number of scattering elements  $N_S$  increases. In particular, Fig. 2(d) shows that the equivalent channel can be completely nulled (corresponding to the origin) by a 128-element BD-RIS thanks to its superior channel shaping capability, but not by a diagonal one. Those results demonstrate the superior channel shaping capability of BD-RIS and emphasizes the importance of reconfigurable inter-connection between elements.

2) *Analytical Bounds and Numerical Results*: Fig. 3 illustrates the analytical singular value bounds in Proposition 2 and the numerical results obtained by solving problem (21) with  $\rho_n = \pm 1$  and  $\rho_{n'} = 0, \forall n' \neq n$ . Here we assume a rank- $k$  forward channel without loss of generality. When the RIS is in the vicinity of the transmitter, Figs. 3(a) and 3(b) show that the achievable channel singular values indeed satisfy Corollary 2.1, namely  $\sigma_1(\mathbf{H}) \geq \sigma_1(\mathbf{T})$ ,  $\sigma_2(\mathbf{T}) \leq \sigma_2(\mathbf{H}) \leq \sigma_1(\mathbf{T})$ , etc. It is obvious that BD-RIS can approach those bounds better than diagonal RIS especially for a small  $N_S$ . Another example is given in Fig. 3(c) with rank-2 forward channel. The first two channel singular values are unbounded above and bounded below by the first two singular values of  $\mathbf{T}$ , while the last two singular values

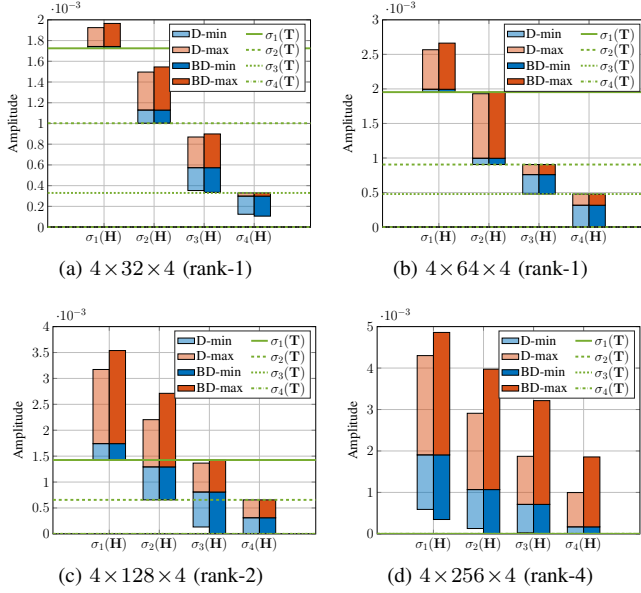


Fig. 3. Achievable channel singular values: analytical bounds (green lines) and numerical optimization results (blue and red bars). The intersections of the blue and red bars denote the singular values of the direct channel. The blue (resp. red) bars are obtained by solving problem (21) with  $\rho_n = -1$  (resp.  $+1$ ) and  $\rho_{n'} = 0, \forall n' \neq n$ . ‘D’ means diagonal RIS and ‘BD’ refers to fully-connected BD-RIS. ‘rank- $k$ ’ refers to the rank of the forward channel.

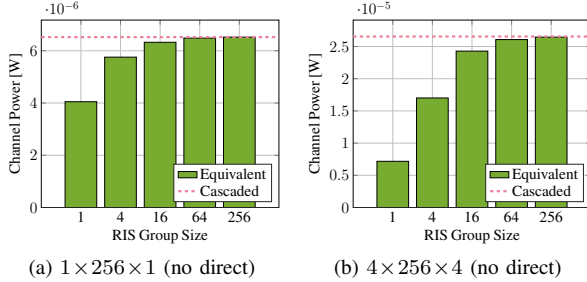


Fig. 4. Average maximum channel power versus BD-RIS group size and MIMO dimensions. The direct channel is blocked. ‘Cascaded’ refers to the available power of the cascaded channel, i.e., the sum of (sorted) element-wise power product of backward and forward channels.

can be suppressed to zero and bounded above by the first two singular values of  $\mathbf{T}$ . Those observations align with Proposition 2. Finally, Fig. 3(d) confirms there are no extra singular value bounds when both forward and backward channels are full-rank. This can be predicted from (25) where the compact singular matrix  $\mathbf{V}_F$  becomes unitary and  $\mathbf{T} = \mathbf{0}$ . The numerical results are consistent with the analytical bounds, and we conclude that the channel shaping advantage of BD-RIS over diagonal RIS scales with forward and backward channel ranks.

Fig. 4 compares the analytical channel power bound in Corollary 3.6 and the numerical results obtained by solving problem (37) when the direct link is blocked. Here, a fully-connected BD-RIS can attain the upper bound either in closed form (34) or via optimization approach (41). For the SISO case in Fig. 4(a), the maximum channel power is approximately  $4 \times 10^{-6}$  by diagonal RIS and  $6.5 \times 10^{-6}$  by fully-connected BD-RIS, corresponding to a 62.5 % gain.

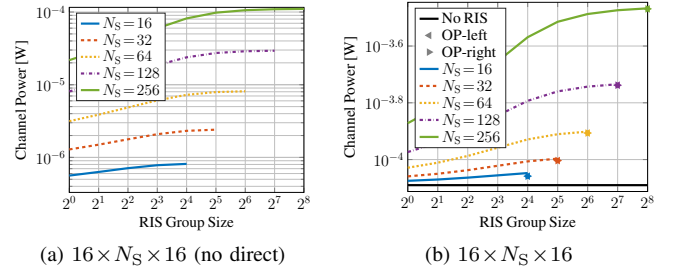


Fig. 5. Average maximum channel power versus RIS configuration. ‘OP-left’ and ‘OP-right’ refer to the suboptimal solutions to problem (37) by lossy transformation (39) where  $\Theta$  is to the left and right of the product, respectively.

This aligns with the asymptotic BD-RIS scaling law derived for SISO in [31]. Interestingly, the gain surges to 270 % in  $N_T = N_S = 4$  MIMO as shown in Fig. 4(b). This is because space alignment boils down to phase matching in SISO such that both triangular and Cauchy-Schwarz inequalities in [31, (50)] can be simultaneously tight regardless of the group size. That is, diagonal RIS is sufficient for space alignment in SISO while the 62.5 % gain from BD-RIS comes purely from channel rearrangement. Now consider a diagonal RIS in MIMO. Each element can only apply a common phase shift to the associated rank-1  $N_R \times N_T$  indirect channel. Therefore, perfect space alignment of indirect channels through different elements is generally impossible. It means the disadvantage of diagonal RIS in space alignment and channel rearrangement scales with MIMO dimensions. We thus conclude that the power gain of BD-RIS scales with group size and MIMO dimensions.

### C. Power Gain and Achievable Rate Maximization

We first focus on channel power gain maximization problem (37). Fig. 5 shows the achievable channel power under different RIS configurations. An interesting observation is that the relative power gain of BD-RIS over diagonal RIS is even larger with direct link. For example, a 64-element fully BD-RIS can almost provide the same channel power as a 256-element diagonal RIS in Fig. 5(b), but not in Fig. 5(a). This is because the RIS needs to balance the multiplicative forward-backward combining and the additive direct-indirect combining, such that the space alignment advantage of BD-RIS becomes more pronounced. We also notice that the suboptimal solutions (40) for fully-connected BD-RIS by lossy transformation (39) are very close to optimal especially for a large  $N_S$ .

Fig. 6 presents the achievable rate under different MIMO and RIS configurations. At a transmit power of 10 dB, Fig. 6(a) shows that introducing a 128-element diagonal RIS to  $N_T = N_S = 4$  MIMO can improve the achievable rate from 22.2 bps/Hz to 29.2 bps/Hz (+31.5 %). In contrast, a BD-RIS of group size 4 and 128 can further improve the rate to 32.1 bps/Hz (+44.6 %) and 34 bps/Hz (+53.2 %), respectively. Interestingly, the gap between the optimal AO approach (44)–(46) and the low-complexity solution (41) and (46) narrows as the group size increases, and completely vanishes for a fully-connected BD-RIS. This implies that the RIS-transceiver design can often be decoupled via channel shaping with marginal performance loss. Figs. 6(b) and 6(c) also confirm the advantage

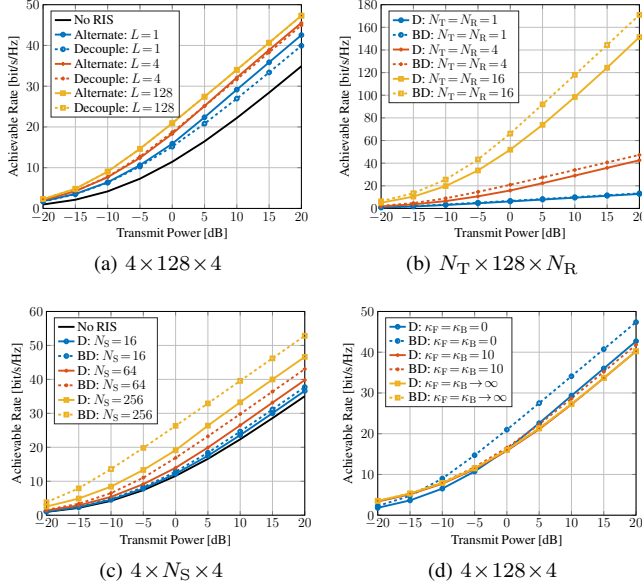


Fig. 6. Average achievable rate versus MIMO and RIS configurations. The noise power is  $\eta = -75$  dB, corresponding to a direct SNR of  $-10$  to  $30$  dB. ‘Alternate’ refers to the alternating optimization and ‘Decouple’ refers to the low-complexity design. ‘D’ means diagonal RIS and ‘BD’ refers to fully-connected BD-RIS.

of BD-RIS grows with the number of transmit and receive antennas and scattering elements. In the low power regime ( $-20$  to  $-10$  dB), the slope of the achievable rate is significantly larger with BD-RIS, suggesting that multiple streams can be activated at a much lower SNR. This is because BD-RIS not only spreads the channel singular values to a wider range, but also provides a better trade-off between channels (c.f. Fig. 2). Finally, Fig. 6(d) shows that the gap between diagonal and BD-RIS narrows as the Rician  $K$ -factor increases and becomes indistinguishable in LoS environment. The observation is expected from previous studies [31], [32], [37] and aligns with Corollary 2.1, which suggests that the BD-RIS should be deployed in rich-scattering environments to exploit its channel shaping potential.

## VII. CONCLUSION

This paper analyzes the channel shaping capability of RIS in terms of singular values redistribution. We consider a general BD architecture that allows elements within the same group to interact, enabling more sophisticated manipulation than diagonal RIS. This translates to a wider dynamic range of and better tradeoff between singular values and significant power and rate gains, especially in large-scale MIMO systems. We characterize the Pareto frontiers of channel singular values via optimization approach and provide analytical bounds for rank-deficient forward/backward channel and blocked direct channel. Specifically, the former is done by proposing an efficient RCG algorithm for BD-RIS optimization problems, which offers better objective value and faster convergence than existing methods. We also present two beamforming designs for rate maximization problem, one based on alternating optimization for optimal performance and the other decouples

the RIS-transceiver design for lower complexity. Extensive simulations show that the advantage of BD-RIS stems from its superior space alignment and channel rearrangement capability, which scales with the number of elements, group size, MIMO dimensions, and channel diversity.

## APPENDIX

### A. Proof of Lemma 1

Let  $\mathbf{H} = \sum_n \mathbf{u}_n \sigma_n \mathbf{v}_n^H$  be the compact SVD of the equivalent channel. Since the singular vectors are orthonormal, the  $n$ -th singular value can be expressed as

$$\sigma_n = \mathbf{u}_n^H \mathbf{H} \mathbf{v}_n = \mathbf{u}_n^T \mathbf{H}^* \mathbf{v}_n^*, \quad (47)$$

whose differential with respect to  $\Theta_g^*$  is

$$\begin{aligned} \partial \sigma_n &= \partial \mathbf{u}_n^T \underbrace{\mathbf{H}^* \mathbf{v}_n^*}_{\sum_m \mathbf{u}_m^* \sigma_m \mathbf{v}_m^T \mathbf{v}_n} + \mathbf{u}_n^T \cdot \partial \mathbf{H}^* \cdot \mathbf{v}_n^* + \underbrace{\mathbf{u}_n^T \mathbf{H}^*}_{\mathbf{u}_n^T \sum_m \mathbf{u}_m^* \sigma_m \mathbf{v}_m^T} \partial \mathbf{v}_n^* \\ &= \underbrace{\partial \mathbf{u}_n^T \mathbf{u}_n^*}_{\partial 1=0} \cdot \sigma_n + \mathbf{u}_n^T \cdot \partial \mathbf{H}^* \cdot \mathbf{v}_n^* + \sigma_n \cdot \underbrace{\mathbf{v}_n^T \partial \mathbf{v}_n^*}_{\partial 1=0} \\ &= \mathbf{u}_n^T \mathbf{H}_{B,g}^* \cdot \partial \Theta_g^* \cdot \mathbf{H}_{F,g}^* \mathbf{v}_n^* \\ &= \text{tr}(\mathbf{H}_{F,g}^* \mathbf{v}_n^* \mathbf{u}_n^T \mathbf{H}_{B,g}^* \cdot \partial \Theta_g^*). \end{aligned}$$

According to [54], the corresponding complex derivative is

$$\frac{\partial \sigma_n}{\partial \Theta_g^*} = \mathbf{H}_{B,g}^H \mathbf{u}_n \mathbf{v}_n^H \mathbf{H}_{F,g}^H. \quad (48)$$

A linear combination of (48) yields (22).

### B. Proof of Proposition 1

The scattering matrix of BD-RIS can be decomposed as

$$\Theta = \mathbf{L} \Theta_D \mathbf{R}^H, \quad (49)$$

where  $\Theta_D \in \mathbb{U}^{N_S \times N_S}$  corresponds to diagonal RIS and  $\mathbf{L}, \mathbf{R} \in \mathbb{U}^{N_S \times N_S}$  are block-diagonal matrices of  $L \times L$  unitary blocks. Manipulating  $\mathbf{L}$  and  $\mathbf{R}$  rotates the linear spans of  $\bar{\mathbf{H}}_B \triangleq \mathbf{H}_B \mathbf{L}$  and  $\bar{\mathbf{H}}_F \triangleq \mathbf{R}^H \mathbf{H}_F$  and maintains their rank. On the other hand, there exists a  $\Theta_D$  such that

$$\begin{aligned} \text{rank}(\mathbf{H}_B \Theta_D \mathbf{H}_F) &= \min(\text{rank}(\mathbf{H}_B), \text{rank}(\Theta_D), \text{rank}(\mathbf{H}_F)) \\ &= \min(\text{rank}(\bar{\mathbf{H}}_B), N_S, \text{rank}(\bar{\mathbf{H}}_F)) \\ &= \max_{\Theta} \text{rank}(\mathbf{H}_B \Theta \mathbf{H}_F) \end{aligned}$$

The same result holds if the direct link is present.

### C. Proof of Proposition 2

We consider rank- $k$  forward channel and the proof follows similarly for rank- $k$  backward channel. Let  $\mathbf{H}_F = \mathbf{U}_F \Sigma_F \mathbf{V}_F^H$  be the compact SVD of the forward channel. The channel Gram matrix  $\mathbf{G} \triangleq \mathbf{H} \mathbf{H}^H$  can be written as

$$\begin{aligned} \mathbf{G} &= \mathbf{H}_D \mathbf{H}_D^H + \mathbf{H}_B \Theta \mathbf{U}_F \Sigma_F \Sigma_F^H \mathbf{U}_F^H \Theta^H \mathbf{H}_B^H \\ &\quad + \mathbf{H}_B \Theta \mathbf{U}_F \Sigma_F \mathbf{V}_F^H \mathbf{H}_D^H + \mathbf{H}_D \mathbf{V}_F \Sigma_F \mathbf{U}_F^H \Theta^H \mathbf{H}_B^H \\ &= \mathbf{H}_D (\mathbf{I} - \mathbf{V}_F \mathbf{V}_F^H) \mathbf{H}_D^H \\ &\quad + (\mathbf{H}_B \Theta \mathbf{U}_F \Sigma_F + \mathbf{H}_D \mathbf{V}_F) (\Sigma_F \mathbf{U}_F^H \Theta^H \mathbf{H}_B^H + \mathbf{V}_F^H \mathbf{H}_D^H) \\ &= \mathbf{Y} + \mathbf{Z} \mathbf{Z}^H, \end{aligned}$$

where we define  $\mathbf{Y} \triangleq \mathbf{H}_D(\mathbf{I} - \mathbf{V}_F \mathbf{V}_F^H) \mathbf{H}_D^H \in \mathbb{H}^{N_R \times N_R}$  and  $\mathbf{Z} \triangleq \mathbf{H}_B \mathbf{\Theta} \mathbf{U}_F \mathbf{\Sigma}_F + \mathbf{H}_D \mathbf{V}_F \in \mathbb{C}^{N_R \times k}$ . That is to say,  $\mathbf{G}$  can be expressed as a Hermitian matrix plus  $k$  rank-1 perturbations. According to the Cauchy interlacing formula [66], the  $n$ -th eigenvalue of  $\mathbf{G}$  is bounded by

$$\lambda_n(\mathbf{G}) \leq \lambda_{n-k}(\mathbf{Y}), \quad \text{if } n > k, \quad (50)$$

$$\lambda_n(\mathbf{G}) \geq \lambda_n(\mathbf{Y}), \quad \text{if } n < N - k + 1. \quad (51)$$

Since  $\mathbf{Y} = \mathbf{T} \mathbf{T}^H$  is positive semi-definite, taking the square roots of (50) and (51) gives (24a) and (24b).

#### D. Proof of Proposition 3

Let  $\mathbf{H}_B = \mathbf{U}_B \mathbf{\Sigma}_B \mathbf{V}_B^H$  and  $\mathbf{H}_F = \mathbf{U}_F \mathbf{\Sigma}_F \mathbf{V}_F^H$  be the SVD of the backward and forward channels, respectively. The scattering matrix of fully-connected BD-RIS can be decomposed as

$$\mathbf{\Theta} = \mathbf{V}_B \mathbf{X} \mathbf{U}_F^H, \quad (52)$$

where  $\mathbf{X} \in \mathbb{U}^{N_S \times N_S}$  is a unitary matrix to be designed. The equivalent channel is thus a function of  $\mathbf{X}$

$$\mathbf{H} = \mathbf{H}_B \mathbf{\Theta} \mathbf{H}_F = \mathbf{U}_B \mathbf{\Sigma}_B \mathbf{X} \mathbf{\Sigma}_F \mathbf{V}_F^H. \quad (53)$$

Since  $\text{sv}(\mathbf{U} \mathbf{A} \mathbf{V}^H) = \text{sv}(\mathbf{A})$  for unitary  $\mathbf{U}$  and  $\mathbf{V}$ , we have

$$\begin{aligned} \text{sv}(\mathbf{H}) &= \text{sv}(\mathbf{U}_B \mathbf{\Sigma}_B \mathbf{X} \mathbf{\Sigma}_F \mathbf{V}_F^H) \\ &= \text{sv}(\mathbf{\Sigma}_B \mathbf{X} \mathbf{\Sigma}_F) \\ &= \text{sv}(\bar{\mathbf{U}}_B \mathbf{\Sigma}_B \bar{\mathbf{V}}_B^H \bar{\mathbf{U}}_F \mathbf{\Sigma}_F \bar{\mathbf{V}}_F^H) \\ &= \text{sv}(\mathbf{B} \mathbf{F}), \end{aligned}$$

where  $\bar{\mathbf{U}}_{B/F}$  and  $\bar{\mathbf{V}}_{B/F}$  are arbitrary unitary matrices.

#### E. Proof of Lemma 2

The differential of  $R$  with respect to  $\mathbf{\Theta}_g^*$  is [54]

$$\begin{aligned} \partial R &= \frac{1}{\eta} \text{tr} \left\{ \partial \mathbf{H}^* \cdot \mathbf{Q}^T \mathbf{H}^T \left( \mathbf{I} + \frac{\mathbf{H}^* \mathbf{Q}^T \mathbf{H}^T}{\eta} \right)^{-1} \right\} \\ &= \frac{1}{\eta} \text{tr} \left\{ \mathbf{H}_{B,g}^* \cdot \partial \mathbf{\Theta}_g^* \cdot \mathbf{H}_{F,g}^* \mathbf{Q}^T \mathbf{H}^T \left( \mathbf{I} + \frac{\mathbf{H}^* \mathbf{Q}^T \mathbf{H}^T}{\eta} \right)^{-1} \right\} \\ &= \frac{1}{\eta} \text{tr} \left\{ \mathbf{H}_{F,g}^* \mathbf{Q}^T \mathbf{H}^T \left( \mathbf{I} + \frac{\mathbf{H}^* \mathbf{Q}^T \mathbf{H}^T}{\eta} \right)^{-1} \mathbf{H}_{B,g}^* \cdot \partial \mathbf{\Theta}_g^* \right\}, \end{aligned}$$

and the corresponding complex derivative is (45).

#### F. Proof of Proposition 4

The differential of (37a) with respect to  $\mathbf{\Theta}_g^*$  is

$$\begin{aligned} \partial \|\mathbf{H}\|_F^2 &= \text{tr}(\mathbf{H}_{B,g}^* \cdot \partial \mathbf{\Theta}_g^* \cdot \mathbf{H}_{F,g}^* (\mathbf{H}_D^T + \mathbf{H}_F^T \mathbf{\Theta}^T \mathbf{H}_B^T)) \\ &= \text{tr}(\mathbf{H}_{F,g}^* (\mathbf{H}_D^T + \mathbf{H}_F^T \mathbf{\Theta}^T \mathbf{H}_B^T) \mathbf{H}_{B,g}^* \cdot \partial \mathbf{\Theta}_g^*) \end{aligned}$$

and the corresponding complex derivative is

$$\frac{\partial \|\mathbf{H}\|_F^2}{\partial \mathbf{\Theta}_g^*} = \mathbf{H}_{B,g}^H (\mathbf{H}_D + \mathbf{H}_B \mathbf{\Theta} \mathbf{H}_F) \mathbf{H}_{F,g}^H = \mathbf{M}_g. \quad (54)$$

First, we approximate the quadratic objective (37a) by its local Taylor expansion

$$\max_{\mathbf{\Theta}} \sum_g 2\Re\{\text{tr}(\mathbf{\Theta}_g^H \mathbf{M}_g)\} \quad (55a)$$

$$\text{s.t.} \quad \mathbf{\Theta}_g^H \mathbf{\Theta}_g = \mathbf{I}, \quad \forall g. \quad (55b)$$

Let  $\mathbf{M}_g = \mathbf{U}_g \mathbf{\Sigma}_g \mathbf{V}_g^H$  be the compact SVD of  $\mathbf{M}_g$ . We have

$$\Re\{\text{tr}(\mathbf{\Theta}_g^H \mathbf{M}_g)\} = \Re\{\text{tr}(\mathbf{\Sigma}_g \mathbf{V}_g^H \mathbf{\Theta}_g^H \mathbf{U}_g)\} \leq \text{tr}(\mathbf{\Sigma}_g). \quad (56)$$

The upper bound is tight when  $\mathbf{V}_g^H \mathbf{\Theta}_g^H \mathbf{U}_g = \mathbf{I}$ , which implies the optimal solution of (55) is  $\tilde{\mathbf{\Theta}}_g = \mathbf{U}_g \mathbf{V}_g^H, \forall g$ .

Next, we prove that solving (55) successively does not decrease (37a). Since  $\tilde{\mathbf{\Theta}}$  optimal for problem (55), we have  $\sum_g 2\Re\{\text{tr}(\tilde{\mathbf{\Theta}}_g^H \mathbf{M}_g)\} \geq \sum_g 2\Re\{\text{tr}(\mathbf{\Theta}_g^H \mathbf{M}_g)\}$  which is explicitly expressed by (58). On the other hand, expanding  $\|\sum_g \mathbf{H}_{B,g} \mathbf{\Theta}_g \mathbf{H}_{F,g} - \sum_g \mathbf{H}_{B,g} \tilde{\mathbf{\Theta}}_g \mathbf{H}_{F,g}\|_F^2 \geq 0$  gives (59). Adding (58) and (59), we have

$$\begin{aligned} &2\Re\{\text{tr}(\tilde{\mathbf{\Theta}}^H \mathbf{H}_B^H \mathbf{H}_D \mathbf{H}_F^H)\} + \text{tr}(\mathbf{H}_F^H \tilde{\mathbf{\Theta}}^H \mathbf{H}_B^H \mathbf{H}_B \tilde{\mathbf{\Theta}} \mathbf{H}_F) \\ &\geq 2\Re\{\text{tr}(\mathbf{\Theta}^H \mathbf{H}_B^H \mathbf{H}_D \mathbf{H}_F^H)\} + \text{tr}(\mathbf{H}_F^H \mathbf{\Theta}^H \mathbf{H}_B^H \mathbf{H}_B \mathbf{\Theta} \mathbf{H}_F), \end{aligned} \quad (57)$$

which suggests that updating  $\tilde{\mathbf{\Theta}}$  does not decrease (37a).

Finally, we prove that the converging point of (55), denoted by  $\mathbf{\Theta}^?$ , is a stationary point of (37). The Karush-Kuhn-Tucker (KKT) conditions of (37) and (55) are equivalent in terms of primal/dual feasibility and complementary slackness, while the stationary conditions are respectively,  $\forall g$ ,

$$\mathbf{H}_{B,g}^H (\mathbf{H}_D + \mathbf{H}_B \mathbf{\Theta}^* \mathbf{H}_F) \mathbf{H}_{F,g}^H - \mathbf{\Theta}_g^* \mathbf{\Lambda}_g^H = 0, \quad (60)$$

$$\mathbf{M}_g - \mathbf{\Theta}_g^* \mathbf{\Lambda}_g^H = 0. \quad (61)$$

On convergence, (61) becomes  $\mathbf{H}_{B,g}^H (\mathbf{H}_D + \mathbf{H}_B \mathbf{\Theta}^? \mathbf{H}_F) \mathbf{H}_{F,g}^H - \mathbf{\Theta}_g^? \mathbf{\Lambda}_g^H = 0$  and reduces to (60). The proof is thus completed.

#### REFERENCES

- [1] E. Basar, M. D. Renzo, J. D. Rosny, M. Debbah, M.-S. Alouini, and R. Zhang, "Wireless communications through reconfigurable intelligent surfaces," *IEEE Access*, vol. 7, pp. 116 753–116 773, 2019.
- [2] Q. Wu and R. Zhang, "Intelligent reflecting surface enhanced wireless network via joint active and passive beamforming," *IEEE Transactions on Wireless Communications*, vol. 18, pp. 5394–5409, Nov 2019.
- [3] H. Guo, Y.-C. Liang, J. Chen, and E. G. Larsson, "Weighted sum-rate maximization for reconfigurable intelligent surface aided wireless networks," *IEEE Transactions on Wireless Communications*, vol. 19, pp. 3064–3076, May 2020.
- [4] Y. Liu, Y. Zhang, X. Zhao, S. Geng, P. Qin, and Z. Zhou, "Dynamic-controlled RIS assisted multi-user MISO downlink system: Joint beamforming design," *IEEE Transactions on Green Communications and Networking*, vol. 6, pp. 1069–1081, Jun 2022.
- [5] Y. He, Y. Cai, H. Mao, and G. Yu, "RIS-assisted communication radar coexistence: Joint beamforming design and analysis," *IEEE Journal on Selected Areas in Communications*, vol. 40, pp. 2131–2145, Jul 2022.
- [6] H. Luo, R. Liu, M. Li, Y. Liu, and Q. Liu, "Joint beamforming design for RIS-assisted integrated sensing and communication systems," *IEEE Transactions on Vehicular Technology*, vol. 71, pp. 13 393–13 397, Dec 2022.
- [7] M. Hua, Q. Wu, C. He, S. Ma, and W. Chen, "Joint active and passive beamforming design for IRS-aided radar-communication," *IEEE Transactions on Wireless Communications*, vol. 22, pp. 2278–2294, Apr 2023.
- [8] Q. Wu and R. Zhang, "Joint active and passive beamforming optimization for intelligent reflecting surface assisted SWIPT under QoS constraints," *IEEE Journal on Selected Areas in Communications*, vol. 38, no. 8, pp. 1735–1748, Aug 2020.
- [9] Z. Feng, B. Clerckx, and Y. Zhao, "Waveform and beamforming design for intelligent reflecting surface aided wireless power transfer: Single-user and multi-user solutions," *IEEE Transactions on Wireless Communications*, 2022.
- [10] Y. Zhao, B. Clerckx, and Z. Feng, "IRS-aided SWIPT: Joint waveform, active and passive beamforming design under nonlinear harvester model," *IEEE Transactions on Communications*, vol. 70, pp. 1345–1359, 2022.
- [11] E. Basar, M. Wen, R. Mesleh, M. D. Renzo, Y. Xiao, and H. Haas, "Index modulation techniques for next-generation wireless networks," *IEEE Access*, vol. 5, pp. 16 693–16 746, Aug 2017.

$$2\Re\left\{\sum_g \text{tr}(\tilde{\Theta}_g^H \mathbf{H}_{B,g}^H \mathbf{H}_D \mathbf{H}_{F,g}^H) + \sum_{g_1, g_2} \text{tr}(\tilde{\Theta}_{g_1}^H \mathbf{H}_{B,g_1}^H \mathbf{H}_{B,g_2} \Theta_{g_2} \mathbf{H}_{F,g_2}^H \mathbf{H}_{F,g_1}^H)\right\} \geq 2\Re\left\{\sum_g \text{tr}(\Theta_g^H \mathbf{H}_{B,g}^H \mathbf{H}_D \mathbf{H}_{F,g}^H) + \sum_{g_1, g_2} \text{tr}(\Theta_{g_1}^H \mathbf{H}_{B,g_1}^H \mathbf{H}_{B,g_2} \Theta_{g_2} \mathbf{H}_{F,g_2}^H \mathbf{H}_{F,g_1}^H)\right\} \quad (58)$$

$$\sum_{g_1, g_2} \text{tr}(\mathbf{H}_{F,g_1}^H \tilde{\Theta}_{g_1}^H \mathbf{H}_{B,g_1}^H \mathbf{H}_{B,g_2} \tilde{\Theta}_{g_2} \mathbf{H}_{F,g_2}) - 2\Re\left\{\sum_{g_1, g_2} \text{tr}(\mathbf{H}_{F,g_1}^H \tilde{\Theta}_{g_1}^H \mathbf{H}_{B,g_1}^H \mathbf{H}_{B,g_2} \Theta_{g_2} \mathbf{H}_{F,g_2})\right\} + \sum_{g_1, g_2} \text{tr}(\mathbf{H}_{F,g_1}^H \Theta_{g_1}^H \mathbf{H}_{B,g_1}^H \mathbf{H}_{B,g_2} \Theta_{g_2} \mathbf{H}_{F,g_2}) \geq 0 \quad (59)$$

- [12] R. Karasik, O. Simeone, M. D. Renzo, and S. S. Shitz, "Beyond max-SNR: Joint encoding for reconfigurable intelligent surfaces," in *2020 IEEE International Symposium on Information Theory (ISIT)*, Jun 2020, pp. 2965–2970.
- [13] E. Basar, "Reconfigurable intelligent surface-based index modulation: A new beyond MIMO paradigm for 6G," *IEEE Transactions on Communications*, vol. 68, pp. 3187–3196, May 2020.
- [14] J. Ye, S. Guo, S. Dang, B. Shihada, and M.-S. Alouini, "On the capacity of reconfigurable intelligent surface assisted MIMO symbiotic communications," *IEEE Transactions on Wireless Communications*, vol. 21, pp. 1943–1959, Mar 2022.
- [15] Y.-C. Liang, Q. Zhang, E. G. Larsson, and G. Y. Li, "Symbiotic radio: Cognitive backscattering communications for future wireless networks," *IEEE Transactions on Cognitive Communications and Networking*, vol. 6, pp. 1242–1255, Dec 2020.
- [16] Y. Zhao and B. Clerckx, "RIScatter: Unifying backscatter communication and reconfigurable intelligent surface," *IEEE Journal on Selected Areas in Communications*, pp. 1–1, Dec 2024.
- [17] H. Yang, H. Ding, K. Cao, M. Elkashlan, H. Li, and K. Xin, "A RIS-segmented symbiotic ambient backscatter communication system," *IEEE Transactions on Vehicular Technology*, vol. 73, pp. 812–825, Jan 2024.
- [18] E. Basar, "Reconfigurable intelligent surfaces for doppler effect and multipath fading mitigation," *Frontiers in Communications and Networks*, vol. 2, May 2021.
- [19] E. Arslan, I. Yildirim, F. Kilinc, and E. Basar, "Over-the-air equalization with reconfigurable intelligent surfaces," *IET Communications*, vol. 16, pp. 1486–1497, Aug 2022.
- [20] O. Ozdogan, E. Bjornson, and E. G. Larsson, "Using intelligent reflecting surfaces for rank improvement in MIMO communications," in *ICASSP 2020 - 2020 IEEE International Conference on Acoustics, Speech and Signal Processing (ICASSP)*, May 2020, pp. 9160–9164.
- [21] Y. Yang, B. Zheng, S. Zhang, and R. Zhang, "Intelligent reflecting surface meets OFDM: Protocol design and rate maximization," *IEEE Transactions on Communications*, vol. 68, pp. 4522–4535, Jul 2020.
- [22] G. Chen and Q. Wu, "Fundamental limits of intelligent reflecting surface aided multiuser broadcast channel," *IEEE Transactions on Communications*, vol. 71, pp. 5904–5919, Oct 2023.
- [23] M. A. ElMossallamy, H. Zhang, R. Sultan, K. G. Seddik, L. Song, G. Y. Li, and Z. Han, "On spatial multiplexing using reconfigurable intelligent surfaces," *IEEE Wireless Communications Letters*, vol. 10, pp. 226–230, Feb 2021.
- [24] S. Meng, W. Tang, W. Chen, J. Lan, Q. Y. Zhou, Y. Han, X. Li, and S. Jin, "Rank optimization for MIMO channel with RIS: Simulation and measurement," *IEEE Wireless Communications Letters*, vol. 13, pp. 437–441, Feb 2024.
- [25] Y. Zheng, T. Lin, and Y. Zhu, "Passive beamforming for IRS-assisted MU-MIMO systems with one-bit ADCs: An SER minimization design approach," *IEEE Communications Letters*, vol. 26, pp. 1101–1105, May 2022.
- [26] W. Huang, B. Lei, S. He, C. Kai, and C. Li, "Condition number improvement of IRS-aided near-field MIMO channels," in *2023 IEEE International Conference on Communications Workshops (ICC Workshops)*, May 2023, pp. 1210–1215.
- [27] A. H. Bafghi, V. Jamali, M. Nasiri-Kenari, and R. Schober, "Degrees of freedom of the K-user interference channel assisted by active and passive IRSs," *IEEE Transactions on Communications*, vol. 70, pp. 3063–3080, May 2022.
- [28] S. Zheng, B. Lv, T. Zhang, Y. Xu, G. Chen, R. Wang, and P. C. Ching, "On DoF of active RIS-assisted MIMO interference channel with arbitrary antenna configurations: When will RIS help?" *IEEE Transactions on Vehicular Technology*, Dec 2023.
- [29] S. H. Chae and K. Lee, "Cooperative communication for the rank-deficient MIMO interference channel with a reconfigurable intelligent surface," *IEEE Transactions on Wireless Communications*, vol. 22, pp. 2099–2112, Mar 2023.
- [30] S. Shen and B. Clerckx, "Beamforming optimization for MIMO wireless power transfer with nonlinear energy harvesting: RF combining versus DC combining," *IEEE Transactions on Wireless Communications*, vol. 20, pp. 199–213, Jan 2021.
- [31] S. Shen, B. Clerckx, and R. Murch, "Modeling and architecture design of reconfigurable intelligent surfaces using scattering parameter network analysis," *IEEE Transactions on Wireless Communications*, vol. 21, pp. 1229–1243, Feb 2022.
- [32] M. Nerini, S. Shen, and B. Clerckx, "Closed-form global optimization of beyond diagonal reconfigurable intelligent surfaces," *IEEE Transactions on Wireless Communications*, vol. 23, pp. 1037–1051, Feb 2024.
- [33] M. Nerini, S. Shen, H. Li, and B. Clerckx, "Beyond diagonal reconfigurable intelligent surfaces utilizing graph theory: Modeling, architecture design, and optimization," *IEEE Transactions on Wireless Communications*, pp. 1–1, May 2024.
- [34] I. Santamaria, M. Soleymani, E. Jorswieck, and J. Gutiérrez, "SNR maximization in beyond diagonal RIS-assisted single and multiple antenna links," *IEEE Signal Processing Letters*, vol. 30, pp. 923–926, 2023.
- [35] —, "Interference leakage minimization in RIS-assisted MIMO interference channels," in *ICASSP 2023 - 2023 IEEE International Conference on Acoustics, Speech and Signal Processing (ICASSP)*, vol. 39, Jun 2023, pp. 1–5.
- [36] H.-R. Ahn, *Asymmetric Passive Components in Microwave Integrated Circuits*. Hoboken, NJ, USA: Wiley, 2006.
- [37] H. Li, S. Shen, and B. Clerckx, "Beyond diagonal reconfigurable intelligent surfaces: From transmitting and reflecting modes to single-, group-, and fully-connected architectures," *IEEE Transactions on Wireless Communications*, vol. 22, pp. 2311–2324, Apr 2023.
- [38] —, "Beyond diagonal reconfigurable intelligent surfaces: A multi-sector mode enabling highly directional full-space wireless coverage," *IEEE Journal on Selected Areas in Communications*, vol. 41, pp. 2446–2460, Aug 2023.
- [39] H. Li, S. Shen, Y. Zhang, and B. Clerckx, "Channel estimation and beamforming for beyond diagonal reconfigurable intelligent surfaces," *arXiv:2403.18087*, 2024.
- [40] H. Li, S. Shen, M. Nerini, M. D. Renzo, and B. Clerckx, "Beyond diagonal reconfigurable intelligent surfaces with mutual coupling: Modeling and optimization," *IEEE Communications Letters*, pp. 1–1, Oct 2024.
- [41] H. Li, M. Nerini, S. Shen, and B. Clerckx, "Wideband modeling and beamforming for beyond diagonal reconfigurable intelligent surfaces," *arXiv:2403.12893*, 2024.
- [42] T. Fang and Y. Mao, "A low-complexity beamforming design for beyond-diagonal RIS aided multi-user networks," *IEEE Communications Letters*, pp. 1–1, Jul 2023.
- [43] Y. Zhou, Y. Liu, H. Li, Q. Wu, S. Shen, and B. Clerckx, "Optimizing power consumption, energy efficiency and sum-rate using beyond diagonal RIS — a unified approach," *IEEE Transactions on Wireless Communications*, pp. 1–1, 2023.
- [44] M. Soleymani, I. Santamaria, E. Jorswieck, and B. Clerckx, "Optimization of rate-splitting multiple access in beyond diagonal RIS-assisted URLLC systems," *IEEE Transactions on Wireless Communications*, pp. 1–1, Jul 2024.
- [45] G. Bartoli, A. Abrardo, N. Decarli, D. Dardari, and M. D. Renzo, "Spatial multiplexing in near field MIMO channels with reconfigurable intelligent surfaces," *IET Signal Processing*, vol. 17, Mar 2023.
- [46] A. Mishra, Y. Mao, C. D'Andrea, S. Buzzi, and B. Clerckx, "Transmitter side beyond-diagonal reconfigurable intelligent surface for massive MIMO networks," *IEEE Wireless Communications Letters*, vol. 13, pp. 352–356, Feb 2024.
- [47] M. Nerini, S. Shen, and B. Clerckx, "Discrete-value group and fully connected architectures for beyond diagonal reconfigurable intelligent surfaces," *IEEE Transactions on Vehicular Technology*, vol. 72, pp. 16 354–16 368, Dec 2023.
- [48] T. E. Abrudan, J. Eriksson, and V. Koivunen, "Steepest descent algorithms for optimization under unitary matrix constraint," *IEEE Transactions on Signal Processing*, vol. 56, pp. 1134–1147, Mar 2008.
- [49] T. Abrudan, J. Eriksson, and V. Koivunen, "Conjugate gradient algorithm for optimization under unitary matrix constraint," *Signal Processing*, vol. 89, pp. 1704–1714, Sep 2009.

- [50] P.-A. Absil, R. Mahony, and R. Sepulchre, *Optimization Algorithms on Matrix Manifolds*. Princeton, NJ, USA: Princeton University Press, 2009.
- [51] C. Pan, G. Zhou, K. Zhi, S. Hong, T. Wu, Y. Pan, H. Ren, M. D. Renzo, A. L. Swindlehurst, R. Zhang, and A. Y. Zhang, "An overview of signal processing techniques for RIS/IRS-aided wireless systems," *IEEE Journal of Selected Topics in Signal Processing*, vol. 16, pp. 883–917, Aug 2022.
- [52] M. T. Ivrlac and J. A. Nossek, "Toward a circuit theory of communication," *IEEE Transactions on Circuits and Systems I: Regular Papers*, vol. 57, pp. 1663–1683, Jul 2010.
- [53] P. Almers, F. Tufvesson, and A. Molisch, "Keyhole effect in mimo wireless channels: Measurements and theory," *IEEE Transactions on Wireless Communications*, vol. 5, pp. 3596–3604, Dec 2006.
- [54] A. Hjørungnes and D. Gesbert, "Complex-valued matrix differentiation: Techniques and key results," *IEEE Transactions on Signal Processing*, vol. 55, pp. 2740–2746, Jun 2007.
- [55] J. Nocedal and S. J. Wright, *Numerical Optimization*. Springer, Sep 2006.
- [56] L. Armijo, "Minimization of functions having lipschitz continuous first partial derivatives," *Pacific Journal of Mathematics*, vol. 16, pp. 1–3, Jan 1966.
- [57] A. Edelman, T. A. Arias, and S. T. Smith, "The geometry of algorithms with orthogonality constraints," *SIAM Journal on Matrix Analysis and Applications*, vol. 20, pp. 303–353, Jan 1998.
- [58] C. Moler and C. V. Loan, "Nineteen dubious ways to compute the exponential of a matrix, twenty-five years later," *SIAM Review*, vol. 45, pp. 3–49, Jan 2003.
- [59] D. Semmler, M. Joham, and W. Utschick, "High SNR analysis of RIS-aided MIMO broadcast channels," in *2023 IEEE 24th International Workshop on Signal Processing Advances in Wireless Communications (SPAWC)*, Sep 2023, pp. 221–225.
- [60] W. Fulton, "Eigenvalues, invariant factors, highest weights, and schubert calculus," *Bulletin of the American Mathematical Society*, vol. 37, pp. 209–249, Apr 2000.
- [61] R. Bhatia, "Linear algebra to quantum cohomology: The story of alfred horn's inequalities," *The American Mathematical Monthly*, vol. 108, pp. 289–318, Apr 2001.
- [62] L. Hogben, Ed., *Handbook of Linear Algebra*. Boca Raton, FL, USA: CRC press, 2013.
- [63] A. Zanella, M. Chiani, and M. Win, "On the marginal distribution of the eigenvalues of wishart matrices," *IEEE Transactions on Communications*, vol. 57, pp. 1050–1060, Apr 2009.
- [64] J. C. Gower and G. B. Dijksterhuis, *Procrustes Problems*. Oxford, UK: Oxford University Press, 2004.
- [65] T. Bell, "Global positioning system-based attitude determination and the orthogonal procrustes problem," *Journal of Guidance, Control, and Dynamics*, vol. 26, pp. 820–822, Sep 2003.
- [66] G. H. Golub and C. F. V. Loan, *Matrix Computations*. Baltimore, MD, USA: Johns Hopkins University Press, 2013.
- [67] F. Nie, R. Zhang, and X. Li, "A generalized power iteration method for solving quadratic problem on the Stiefel manifold," *Science China Information Sciences*, vol. 60, p. 112101, Nov 2017.
- [68] B. Clerckx and C. Oestges, *MIMO Wireless Networks: Channels, Techniques and Standards for Multi-Antenna, Multi-User and Multi-Cell Systems*. Waltham, MA, USA: Academic Press, 2013.
- [69] D. Tse and P. Viswanath, *Fundamentals of Wireless Communication*. Cambridge, UK: Cambridge University Press, May 2005.